JNeurosci
THE JOURNAL OF NEUROSCIENCE

Research Articles: Systems/Circuits

Sexually dimorphic neurosteroid synthesis regulates neuronal activity in the murine brain

https://doi.org/10.1523/JNEUROSCI.0885-21.2021

Cite as: J. Neurosci 2021; 10.1523/JNEUROSCI.0885-21.2021

Received: 22 April 2021
Revised: 12 August 2021
Accepted: 10 September 2021

Sexually dimorphic neurosteroid synthesis regulates neuronal activity in the murine brain

Philipp Wartenberg[1], Imre Farkas[2], Veronika Csillag[3,4], William H. Colledge[5], Erik Hrabovszky[2] and Ulrich Boehm[1]

[1]Experimental Pharmacology, Center for Molecular Signaling (PZMS), Saarland University School of Medicine, Homburg, Germany; [2]Laboratory of Reproductive Neurobiology, Institute of Experimental Medicine, Budapest, Hungary; [3]Laboratory of Endocrine Neurobiology Institute of Experimental Medicine, Budapest, Hungary, [4]Tamás Roska Doctoral School Péter Pázmány Catholic University, Budapest, Hungary, [5]Department of Physiology, Development and Neuroscience, University of Cambridge, Cambridge, UK

Abbreviated title: Neurosteroids regulate neuronal activity.

Key terms: *aromatase, kisspeptin, estrogen receptor, arcuate nucleus, hypothalamus, amygdala, neural circuits, in utero, patch clamp, slice electrophysiology, Cre recombinase, τGFP*

Number of figures: 9; ***Number of tables:*** 1; ***Number of extended figures:*** 2; ***Number of extended tables:*** 11

Number of words Abstract: 152, ***Number of words Introduction:*** 601, ***Number of words Discussion:*** 1078

Corresponding authors and persons to whom reprint requests should be addressed:

Ulrich Boehm, PhD
Experimental Pharmacology, Center for Molecular Signaling (PZMS),
Saarland University School of Medicine, Kirrbergerstrasse/Building 61.4,
66421 Homburg, Germany
Phone: +-49-6841-16-47879
Fax: +-49-6841-16-47934
e-mail: ulrich.boehm@uks.eu

Erik Hrabovszky
Laboratory of Reproductive Neurobiology
Institute of Experimental Medicine

1083 Budapest, Hungary
Phone: +-36-1-210-9400
e-mail: hrabovszky.erik@koki.hu

Grants: Deutsche Forschungsgemeinschaft (DFG) SFB 894 and SFB/TR152 to Ulrich Boehm and the National Science Foundation of Hungary (K128317, K138137) and the Hungarian Brain Research Program (2017-1.2.1-NKP-2017-00002) to Erik Hrabovszky.

Disclosure statement: The authors have nothing to disclose.

Acknowledgements: The authors would like to thank Nirao Shah (Stanford University, CA, USA) for providing the Aromatase-IRES-Cre mice. This project was supported by the Deutsche Forschungsgemeinschaft (DFG) through grants to Ulrich Boehm (SFB894, SFB/TR152) and the National Science Foundation of Hungary (K128317, K138137) and the Hungarian Brain Research Program (2017-1.2.1-NKP-2017-00002) to Erik Hrabovszky

ABSTRACT

Sex steroid hormones act on hypothalamic kisspeptin neurons to regulate reproductive neural circuits in the brain. Kisspeptin neurons start to express estrogen receptors (ERs) *in utero*, suggesting steroid hormone action on these cells early during development. Whether neurosteroids are locally produced in the embryonic brain and impinge onto kisspeptin/reproductive neural circuitry is not known. To address this question, we analyzed aromatase expression, a key enzyme in estrogen synthesis, in male and female mouse embryos. We identified an aromatase neuronal network comprising ~6000 neurons in the hypothalamus and amygdala. By birth, this network has become sexually dimorphic in a cluster of aromatase neurons in the arcuate nucleus adjacent to kisspeptin neurons. We demonstrate that male arcuate aromatase neurons convert testosterone to estrogen to regulate kisspeptin neuron activity. We provide spatio-temporal information on aromatase neuronal network development and highlight a novel mechanism whereby aromatase neurons regulate the activity of distinct neuronal populations expressing ERs.

SIGNIFICANCE STATEMENT

Sex steroid hormones such as estradiol are important regulators of neural circuits controlling reproductive physiology in the brain. Embryonic kisspeptin neurons in the hypothalamus express steroid hormone receptors, suggesting hormone action on these cells in utero. Whether neurosteroids are locally produced in the brain and impinge onto reproductive neural circuitry is insufficiently understood. To address this question, we analyzed aromatase expression, a key enzyme in estradiol synthesis, in mouse embryos and identified a network comprising ~6000 neurons in the brain. By birth, this network has become sexually dimorphic in a cluster of aromatase neurons in the arcuate nucleus adjacent to kisspeptin neurons. We demonstrate that male aromatase neurons convert testosterone to estradiol to regulate kisspeptin neuron activity.

INTRODUCTION

Sex steroid hormones are important regulators of the neural circuits controlling reproductive physiology and behavior in the brain (McCarthy, 2008; Micevych and Meisel, 2017; Balthazart, 2020; Ventura-Aquino and Paredes, 2020). Within this neuronal network, sex steroid signals are detected by kisspeptin neurons in the hypothalamus and then relayed to gonadotropin releasing hormone (GnRH) neurons (Pielecka-Fortuna et al., 2008; Lehman et al., 2010; Mayer et al., 2010; Dubois et al., 2015; Yip et al., 2015; Dubois et al., 2016; Wang et al., 2018). GnRH is released from axon terminals in the median eminence at the base of the brain and then acts on gonadotrope cells in the anterior pituitary gland to regulate gonadal function (Glanowska et al., 2012; Candlish et al., 2018). Synaptic communication between kisspeptin and GnRH neurons is established during embryonic development of the murine brain (Kumar et al., 2014; Kumar et al., 2015). Embryonic kisspeptin neurons start to express estrogen receptor α (ERα) in both males and females and androgen receptor (AR) in males, suggesting that the kisspeptin/GnRH neural circuits become steroid-hormone-sensitive *in utero* and raising the possibility that steroid hormones may act on these cells early during development.

Sex steroids are not only gonadal in source but can also be produced locally in the brain (Kenealy et al., 2013; Kenealy et al., 2017). Aromatase is encoded by the Cyp19A1 gene and converts androgen into estrogen (Santen et al., 2009). Aromatase expression has been detected in the brain of different species (Balthazart et al., 1991; Wagner and Morrell, 1997; Sasano et al., 1998; Wacker et al., 2016). Whether neurosteroids are locally produced in the embryonic mouse brain and impinge onto kisspeptin/GnRH neural circuits is not known. At late embryonic stages and during the first days after birth in rodents, estrogen is needed in males to masculinize the brain (Scordalakes and Rissman, 2004; McCarthy, 2008; Wu et al., 2009). Consistent with this, blocking of estrogen access prevents defeminization of the male brain (Vreeburg et al., 1977). During this critical time period, alpha-fetoprotein protects the

embryos from maternal estrogen synthesized in the placenta (Toran-Allerand, 2005; Bakker et al., 2006; De Mees et al., 2007).

Reliable antibodies against aromatase have been difficult to produce due to the enzyme's localization in the membrane of the endoplasmic reticulum. The detection of aromatase mRNA in the brain has been hampered by low expression levels in this tissue. More recently, reporter mouse strains have provided important insights into aromatase expression in the rodent brain (Wu et al., 2009; Stanic et al., 2014). These studies identified aromatase neurons in distinct regions important for sexual and aggressive behavior and reproduction (Unger et al., 2015) and demonstrated that aromatase expression is sexually dimorphic in adults. Aromatase is already expressed in the brain before puberty and is important for the masculinization of the brain (Wu et al., 2009). While previous studies had provided some experimental evidence for aromatase expression in the embryonic rodent brain (Sanghera et al., 1991; Lephart et al., 1992; Lauber and Lichtensteiger, 1994), the individual neurons and the respective neural circuits expressing aromatase *in utero* have remained elusive.

Capitalizing on reporter mice, we find that aromatase is specifically expressed in distinct neurons in the murine forebrain as early as embryonic day 13.5, developing into an aromatase network comprising ~6000 neurons in the hypothalamus and the amygdala *in utero*. At birth, we identified a cluster of aromatase neurons in the arcuate nucleus immediately adjacent to kisspeptin neurons in the male, but not in the female hypothalamus. We demonstrate that testosterone impinges on the firing activity of kisspeptin neurons, likely mediated by estradiol through endogenous aromatization in the brain.

MATERIALS AND METHODS

Experimental Design

We analyzed aromatase expression *in utero* and after birth capitalizing on the Aromatase-IRES-Cre (ArIC) (Unger et al., 2015) knock-in mouse strain crossed with eROSA26-τGFP (eR26-τGFP) (Wen et al., 2011) animals, resulting in ArIC/eR26-τGFP reporter mice. Expression from the *ROSA26* locus results in τGFP exclusively labeling aromatase expressing cells and fibers enabling quantification of τGFP expressing neurons (n = 3-5 for males and n = 3-4 for females). Acute expression of aromatase and other key genes of the esotrgen synthesis chain was analysed by qPCR (n = 3-4 animals per age and sex). Relation of τGFP cells to ERα-expressing cells was investigated by measuring the distance between τGFP and ERα neurons (n = 3 for each sex and age). Whole-cell patch-clamp recordings in kisspeptin neurons were used to investigate the influence of estrogen on kisspeptin neuron firing in 4-7 days old males (n = 33 cells) and females (n = 6 cells, Table 8-1 – 8-3).

Mice

Animal care and experimental procedures were approved by the animal welfare committee of the Saarland University and performed in accordance with their established guidelines. Mice were kept under a standard light/dark cycle (lights on at 7 AM and off at 7 PM) with food and water *ad libitum*. To label aromatase-expressing cells, we crossed ArIC mice with eR26-τGFP animals. In the resulting ArIC/eR26-τGFP mice, Cre recombinase is bicistronically expressed under control of the *Cyp19A1* promotor. Cre-mediated recombination results in the removal of a strong transcriptional stop cassette from the *ROSA26* locus and subsequent constitutive expression of τGFP exclusively labeling aromatase expressing cells and fibers. All animals used in this study were heterozygous for the ArIC and the eR26-τGFP alleles, respectively and analysed at the following developmental stages: embryonic day 12.5 (E12.5), E13.5, E16.5 and E18.5 and at postnatal day 0 (P0).

KP-ZsGreen transgenic mice used for whole-cell patch-clamp electrophysiology were generated by breeding Kiss1-Cre transgenic mice (Yeo et al., 2016) with the Gt(ROSA)26Sor_CAG/LSL_ZsGreen1 Tm indicator strain (The Jackson Laboratory, JAX No. 007906) at the Medical Gene Technology Unit of the Institute of Experimental Medicine, Budapest, Hungary. Newborn (P4-7) male KP-ZsGreen mice heterozygous for the KP-Cre allele were housed in light- (12:12 light-dark cycle, lights on at 06:00 h) and temperature-controlled environment (22 ± 2°C), with free access to standard food and water. All animal studies were carried out with permissions from the Animal Welfare Committee of the IEM (Permission Number: A5769-01) and in accordance with legal requirements of the European Community (Directive 2010/63/EU). Experiments were designed in accord with accepted standards of animal care and all efforts were made to minimize animal suffering.

Tissue preparation

Embryonic tissue was prepared as described previously (Kumar and Boehm, 2014). In brief, pregnant mice were anesthetized and killed, the embryos removed, washed in ice-cold PBS and immersed in 4% paraformaldehyde (PFA) on ice overnight. Whole embryos (E12.5 and E13.5) or embryo heads (E16.5 and E18.5) were then transferred to 30% sucrose and kept at 4°C until they sank. The embryos were frozen in optimal cutting solution (Leica) and 14 µm sagittal sections were prepared using a cryostat. Embryo tail biopsies were digested in lysis buffer, genotyped and used for sex determination by PCR (Agulnik et al., 1997), as described previously (Kumar and Boehm, 2014). At P0, mice were perfused transcardially with 4% PFA under ketamine/xylazine anaesthesia. Brains were removed, postfixed in 4% PFA for 2 hours on ice, transferred to 30% sucrose at 4°C until they sank and frozen in tissue freezing medium (Leica, Nussloch, Germany). Coronal sections (14 µm), were prepared using a cryostat (Leica) and stored at -80ºC until use.

Immunofluorescence

Sections from ArIC/eR26-τGFP mice were incubated in PBS with 10% donkey serum (Jackson Immunoresearch, West Grove, PA, USA), 3% BSA (Sigma, St. Louis, MO, USA) and 0.3% TX-100 for 1 hour at 20-25°C, followed by incubation with chicken anti-GFP antiserum (1:1,000; A10262; Invitrogen, Carlsbad, CA, USA), diluted in PBS at 4°C overnight. Sections were then incubated in goat anti-chicken Alexa 488 (1:500; A11039; Invitrogen) in PBS for 2 hours at 20-25°C. Subsequently, sections were either incubated in primary antisera against ERα (1:1000; 06–935; Millipore, Burlington, MA, USA), diluted in PBS (overnight at 4°C) or against kisspeptin (1:500, AB9754, Millipore, St. Louis, MO, USA), diluted in PBS (48 h at 4°C) and then treated with anti-rabbit IgG antiserum (1:500; 711-165-152; Jackson Immunoresearch), diluted in PBS, for 2 hours at 20-25°C. Nuclei were stained with Hoechst solution (1:10000, Sigma) in PBS for 10 minutes and the sections were mounted with Fluoromount-G (Southern Biotech, Birmingham, ALA, USA). Slides were analyzed on an Axioskop2 microscope equipped with AxioVision software (Zeiss, Jena, Germany) or an Axio Scan.Z1 with Zen-Blue software (Zeiss).

Quantification of neurons

Neurons were manually counted in every fifth section using the ImageJ Cell Counter plugin. τGFP and kisspeptin neurons were counted based on positively stained cytoplasm and ERα neurons were counted based on nuclear signal. Counted numbers were multiplied by 2.5 to estimate the total number of neurons per brain (Boehm et al., 2005). Fiber density was qualitatively determined and grouped in four different categories based on intensity.

ERα distance measurements

Distances between τGFP-positive, but ERα-negative neurons and τGFP-negative/ERα-positive cells were calculated with the line tool in the Zen-Blue software (Zeiss). Randomly chosen cells from three different animals per age and sex group were included in the calculation.

RT-PCR

Total RNA from E12.5, E13.5, E16.5 and E18.5 embryo brains was isolated with the RNeasy Mini Kit (Qiagen) according to the manufacturer's instructions and the RNA concentration was measured using a Nanodrop. Total RNA was treated with DNase (TURBO DNA-free kit, Invitrogen) before cDNA was synthesized using the Maxima First Strand kit (Thermo Fischer) according to manufacturer's instructions. Quantitative RT-PCR reactions with primers against Cyp11a1, Cyp17a1, Cyp19a1 and β-actin were performed using the SensiFAST SYBR No-ROX kit (Bioline). Controls without template and without reverse transcriptase, respectively, were included.

Brain slice preparation

Neonatal male and female KP-ZsGreen mice (P4-7) were killed by decapitation after deep isoflurane anesthesia. The heads were immersed in ice-cold low-Na^+ cutting solution bubbled with carbogen (a mixture of 95% O_2 and 5% CO_2) and the brains were removed rapidly from the skull. The cutting solution contained the following (in mM): saccharose 205, KCl 2.5, $NaHCO_3$ 26, $MgCl_2$ 5, NaH_2PO_4 1.25, $CaCl_2$ 1, glucose 10. Hypothalamic blocks were dissected, and 200 µm-thick coronal slices were prepared with a VT-1000S vibratome (Leica Microsystems, Wetzlar, Germany) in the ice-cold oxygenated cutting solution. Slices including the arcuate nucleus (ARC) were transferred into artificial cerebrospinal fluid (aCSF) containing (in mM): NaCl 130, KCl 3.5, $NaHCO_3$ 26, $MgSO_4$ 1.2, NaH_2PO_4 1.25, $CaCl_2$ 2.5, glucose 10 and allowed to equilibrate for 1 h. The aCSF was bubbled with carbogen and the temperature was allowed to decrease slowly from 33°C to room temperature.

Whole-cell patch-clamp recordings

Recordings were carried out in carbogenated aCSF at 33°C, using an Axopatch-200B patch-clamp amplifier, a Digidata-1322A data acquisition system, and a pCLAMP 10.4 software

(Molecular Devices Co., Silicon Valley, CA, USA). The patch electrodes (OD = 1.5 mm, thin wall; WPI, Worcester, MA, USA) were prepared with a Flaming-Brown P-97 puller (Sutter Instrument Co., Novato, CA, USA). Electrode resistance was 2–3 MΩ. The intracellular pipette solution contained (in mM): K-gluconate 130, KCl 10, NaCl 10, HEPES 10, $MgCl_2$ 0.1, EGTA 1, Mg-ATP 4, Na-GTP 0.3. pH=7.2-7.3 with KOH. Osmolarity was adjusted to 300 mOsm with D-sorbitol. To eliminate any direct androgen receptor-mediated response to testosterone, the androgen receptor blocker flutamide (1 μM; Tocris; Bristol, UK) (Yang et al., 2018) was included in the intracellular pipette solution. Once the whole-cell patch-clamp configuration was achieved, the intracellular milieu was allowed to reach an equilibrium for 15 min before the recording was started. To eliminate indirect transsynaptic actions of testosterone, spike-mediated neurotransmitter release was blocked in all experiments by the addition of the $GABA_A$-R blocker picrotoxin (100 μM, Tocris) and the glutamate-receptor blocker kynurenic-acid (2 mM, Sigma) to the aCSF 10 min before recording. KP-ZsGreen neurons of the Arc were visualized with a BX51WI IR-DIC microscope (Olympus Co., Tokyo, Japan) placed on an antivibration table (Supertech Ltd., Hungary-Switzerland) using a brief illumination at 470 nm and an epifluorescent filter set. Firing was recorded in current-clamp mode with a holding current of 0 pA. Following a 5-min control recording period, aCSF was replaced with aCSF containing 50 nM testosterone (similar to the male serum T concentration (Travison et al., 2017; Kapourchali et al., 2020) or 17β-estradiol (E2) and the recording continued for 10 additional minutes. Other measurements were carried out in the presence of the aromatase-inhibitor letrozole (100 nM, Tocris) (Kretz et al., 2004; Scarduzio et al., 2013) or the broad-spectrum estrogen-receptor antagonist ICI182,780 (Faslodex, 1 μM, Tocris) (Chu et al., 2009; Balint et al., 2016). The blockers were added to the aCSF 15 min before testosterone (i.e. 10 minutes before the control recording started) and were present throughout the recording. In some measurements, letrozole was applied intracellularly (100 nM), together with flutamide (1 μM) to eliminate endogenous aromatase activity that might occur within kisspeptin neurons. Each neuron served as its own control when drug effects were evaluated.

Statistical methods

All data are presented as the mean ± SEM. Two-tailed unpaired Student's *t* tests were used to determine statistical significance in all counting experiments. Patch-clamp recordings were stored and analyzed off-line. Event detection was performed using the Clampfit module of the PClamp 10.4 software (Molecular Devices Co., Silicon Valley, CA, USA). Firing rates within the 10-min treatment periods were presented and then illustrated in the bar graphs as percentages of the firing rate of the 5 min control periods that is all experiments were self-controlled in each neuron. Two-tailed unpaired Student's *t* tests were used to determine statistical significance in each group of these percentage firing rate data. These percentage data characterizing the different treatment groups were then compared by ANOVA, followed by Tukey's post-hoc test. Statistical differences were considered significant at $p < 0.05$.

RESULTS

In utero aromatase expression is initiated in the brain

To identify aromatase neurons in the embryonic mouse brain, we generated reporter mice in which cells activating the promoter of the *Cyp19A1* gene are tagged with τGFP (ArIC/eR26-τGFP; Fig. 1A). The τGFP fusion protein is actively transported along the axonal microtubules (Mombaerts et al., 1996) visualizing both aromatase-positive perikarya and their projections. While we did not find fluorescent signal in either male or female brains at embryonic day 12.5 (E12.5; Fig. 1B), we detected τGFP cells at E13.5 (Fig. 1C and 1D, Table 1-1). The fluorescent cells were restricted to two distinct forebrain nuclei, the preoptic area (46.0 ± 5.6 τGFP cells in males; 48.8 ± 14.9 cells in females) and the *stria terminalis* (17.5 ± 4.2 cells in males; 23.1 ± 6.3 cells in females; n = 4-5 animals), respectively. Both nuclei also contained some τGFP fibers in close apposition to the labeled somata. Of note, fluorescent cells were not apparent in any other tissue of fetuses, demonstrating that *in utero* aromatase expression is restricted to the brain.

Development of an embryonic aromatase neural network

The total number of aromatase neurons increased throughout embryonic brain development to >6000 neurons before birth (E13.5: 63.5 ± 6.2 vs. E16.5: 3921 ± 380.4 vs. E18.5: 6073 ± 324.1 τGFP+ cells in males (n = 3-5 animals) and E13.5: 56.3 ± 12.9 vs. E16.5: 3330 ± 262.2 vs. E18.5: 6583 ± 458.5 cells in females (n = 3-4 animals; Fig. 1B, Table 1). Aromatase expression was restricted to distinct nuclei in the hypothalamus and the amygdala/*stria terminalis* at all stages analysed (Fig. 2). Furthermore, fluorescent cells were not detected in any other embryonic tissues, indicating that *in utero* aromatase expression remains to be restricted to the brain.

At E16.5, most aromatase neurons were identified in the medial amygdaloid nucleus (1047.5 ± 88.8 cells in males, 839.3 ± 83.8 cells in females) and the medial preoptic area (1070.8 ± 178 cells in males, 996.8 ± 70.3 cells in females, n = 3 animals) (Fig. 1B and Table 1-2). Both

nuclei were also decorated with extensive fluorescent fibers (Fig. 1C and 1D). Additional aromatase neurons were detected in the cortical amygdaloid nucleus and in the optic tract. We also found fluorescent somata and dense fibers in the *stria terminalis*, the bed nucleus of the *stria terminalis*, the ventromedial and the dorsomedial nuclei, the paraventricular nucleus and the medial tuberal nucleus. We detected more τGFP+ neurons in the dorsomedial nucleus in female animals when compared to males (unpaired Student's T-test: $p = 0.0258$, Table 1-2). Numerous τGFP fibers were found to be in close contact with other fluorescent somata and/or fibers, suggesting an aromatase neural network (Fig. 1E). A few aromatase neurons were located in the lateral preoptic and the lateral hypothalamic areas, respectively.

At E18.5 (Fig. 1B and F), aromatase expression was picked up in the amygdalohippocampal area (135.8 ± 39.3 cells in males, 150 ± 45.1 cells in females, n=3 animals). A few τGFP fibers were apparent in the amygdalohippocampal area and the cortical amygdaloid nucleus. In contrast, both the optic tract and particularly the medial amygdaloid nucleus contained dense fluorescent fibers, decorating almost the entire nucleus and coming in close contact with numerous aromatase neuron cell bodies (Fig. 1F, Table 1 and Table 1-3). Fluorescent neurons and fibers in the hypothalamus remained restricted to the nuclei identified at E16.5, with somewhat increased cell numbers. Most aromatase neurons were found in the medial preoptic area with 2722.5 ± 123.5 cells in males and 2885 ± 217.4 cells in females ($n = 3$ animals). This individual nucleus also showed the highest increase in tagged cells when compared to E16.5 embryos. In the dorsomedial nucleus more reporter gene expressing neurons were found in females, comparable to E16.5 animals (unpaired Student's T-test: $p = 0.0344$, Table 1-3). The medial tuberal nucleus, the lateral hypothalamic and the lateral preoptic areas only contained sparse fluorescent fibers, whereas the other τGFP nuclei displayed dense τGFP fibers. The *stria terminalis* contained particularly dense fluorescent fibers comparable to the medial amygdaloid nucleus. Of note, we did not pick up any gross sexual dimorphism in the aromatase expression pattern in any nucleus at any embryonic developmental stage analyzed (Fig. 1B).

To corroborate these findings, we performed quantitative RT-PCR for the *Cyp19a1* gene (catalyzing both the conversion of androstendione to estrone and of testosterone to estradiol) and also for other key enzymes in steroid synthesis, the *Cyp11a1* (converting cholesterol to pregnolone) and *Cyp17a1* genes (converting pregnolone to 17 alpha hydroxypregnolone and to 17 alpha hydroxypregnolone dehyroepiandrosterone, DHEA), respectively, in E12.5, E13.5, E16.5 and E18.5 animals of both sexes (Fig. 3). We detected very low amounts of *Cyp19a1* mRNA just above the detection threshold at E12.5 and a trend towards some increase at E13.5. *Cyp19a1* expression then increased substantially at E16.5 (E13.5 *vs.* E16.5 unpaired Student's T-tests: $p = 0.0219$ for females, $p = 0.0064$ for males; $n = 3$-4), consistent with higher numbers of aromatase neurons revealed by genetic labeling at this age.

Cyp11a1 expression levels increased from E12.5 to E13.5 in females (unpaired Student's T-test: $p = 0.0872$, $n = 4$), but not in males. Expression increased further at E16.5 (unpaired Student's T-test: $p = 0.0232$, $n = 3$-4) and remained at this plateau at E18.5. *Cyp17a1* expression increased from E12.5 to E13.5 in females (unpaired Student's T-test: $p = 0.0075$, $n = 4$) with a trend to a further increase at E16.5.

With the sole exception of *Cyp17a1* expression at E13.5, where females expressed more mRNA than males (unpaired Student's T-test: $p = 0.0195$, $n = 3$-4), we did not find age-specific sex differences in expression of these key enzymes in steroid synthesis.

Distinct neural circuits become estrogen-sensitive *in utero*

Aromatase, kisspeptin, GPR54/kisspeptin receptor and estrogen receptor α (ERα) expression all start at E13.5 in the male and female murine brain (Kumar et al., 2014; Kumar et al., 2015), suggesting temporal orchestration and raising the possibility, that locally produced neurosteroids impinge onto estrogen-sensitive neural circuits *in utero*. To characterize the respective circuitry and test whether estrogen-sensitivity may provide an autocrine feedback mechanism in aromatase neurons, we immunolabeled sections prepared from ArIC/eR26-τGFP brains with antibodies against ERα. We focused on ERα in this study as it has been

shown to play a major role in the development and regulation of the reproductive axis (Walker and Korach, 2004; Mayer et al., 2010). We did not detect immunofluorescence signals for ERα in E12.5 embryos (Fig. 4), consistent with previous reports (Kumar et al., 2014; Kumar et al., 2015). While ERα immunoreactivity was apparent in multiple nuclei at E13.5, it did not colocalize with aromatase neurons in females or in males (Fig. 4, Table 4-1). In contrast, ~15% (14.7% ± 0.6% in males, 14.8% ± 0.7% in females, n = 3 animals) of all aromatase neurons expressed ERα at E16.5. Specifically, some colocalization between aromatase and ERα signals was picked up in the amygdala, the optic tract and the *stria terminalis*, while we did not observe ERα expression in most hypothalamic aromatase neurons.

The medial tuberal nucleus exhibited the highest colocalization rate (57.1% ± 12% in males, 44.4% ± 3.2% in females) but contained only few aromatase neurons (Table 4-2). *Vice versa*, the medial preoptic area with the highest number of aromatase neurons only showed a low rate of colocalization (11.4% ± 1.6% in males, 7.6% ± 3.2 in females).

ERα-positive aromatase neurons remained at similarly low frequency at E18.5 (14% ± 0.5% of aromatase neurons in males, 16.7% ± 1.3% in females; Table 4-3). For example, while we did observe intense ERα staining in the optic tract, we found that hardly any τGFP somata overlapped with the ERα population. ERα-positive aromatase neurons increased somewhat in total numbers when compared to E16.5 (unpaired Student's T-tests: $p = 0.0168$ for males and $p = 0.0051$ for females, Table 4-2 and 4-3). Taken together, these data suggest little autocrine estrogen action on aromatase neurons in the embryonic mouse brain via ERα.

Aromatase neurons are in close proximity to estrogen-sensitive circuits

We next investigated the spatial relationship between aromatase and estrogen-sensitive neurons and determined the mean distance between these cells in the medial preoptic area of the hypothalamus. We found average distances corresponding to ~2-3 cell diameters between aromatase and ERα neurons (61.4 μm in males and 50.9 μm in females at E13.5, 44.6 μm in

384 males and 38.9 μm in females at E16.5, 55.2 μm in males and 50.1 μm in females at E18.5).
385 Similar distances were determined in the medial amygdaloid nucleus (26.4 μm in males and
386 25.9 μm in females at E16.5, 47.4 μm in males and 42.9 μm in females at E18.5). Taken
387 together, these data demonstrate that most aromatase neurons are in close proximity to
388 estrogen-sensitive neurons in the embryonic mouse brain and raise the possibility that locally
389 synthesized estrogen acts on adjacent ERα-positive but aromatase-negative cells (Fig. 5).
390
391 **Sexually dimorphic aromatase expression in the arcuate nucleus at birth**
392 Aromatase expression at P0 remained restricted to nuclei of the amygdala and hypothalamus.
393 We detected more aromatase neurons in the female medial preoptic area (unpaired student's
394 T-test: 0.0418) (Figure 6 and Table 6-1). Colocalization rates between aromatase neurons and
395 ERα neurons in P0 animals were also similar to embryonic brains with the majority of nuclei
396 showing no sex differences. Exceptions were the medial division, posteromedial part of the
397 bed nucleus of stria terminalis (26.44 % ± 4.14% in females and 3.81% ± 2.23% in males,
398 unpaired Student's t-test: $p = 0.0018$), the medial amygdaloid nucleus, posterodorsal part
399 (43.83% ± 8.66% in females and 9.52% ± 3.13% in males, unpaired Student's t-test: $p =$
400 0.0390) and the posteromedial cortical amygdaloid nucleus (11.80% ± 4.59% in females and
401 2.66% ± 1.60% in males, unpaired Student's t-test: $p = 0.0390$, Table 6-2).
402 To test the hypothesis that aromatase neurons may act as local producers of estrogen and to
403 determine whether neurosteroids act on reproductive neural circuits just after birth, we
404 analysed the spatial relationship between aromatase and kisspeptin neurons. Kisspeptin
405 neurons are restricted to the arcuate nucleus of the hypothalamus until puberty and express
406 ERα (Kumar et al., 2014; Kumar et al., 2015). We did not detect aromatase neurons in the
407 arcuate nucleus in either males or females throughout embryonic development (Fig. 7, 7-1
408 and 7-2).
409 However, this changed at birth (Fig. 6). At P0, we found a cluster of τGFP neurons in the
410 male arcuate nucleus (176 ± 64.1 τGFP cells, $n = 5$ animals, Table 6-1). This aromatase

neuron cluster was notably absent in the female arcuate nucleus, demonstrating sexually dimorphic aromatase expression in this area of the hypothalamus at birth.

We next stained brains sections prepared from ArIC/eR26-τGFP brains with antibodies against kisspeptin. While none of the arcuate aromatase neurons expressed kisspeptin (Fig. 8 A), these two neuronal subtypes were always in the immediate vicinity of each other, suggesting steroid hormone action on kisspeptin neurons in the male mouse brain at birth (Fig. 9).

Inhibition of arcuate kisspeptin neurons by testosterone requires estrogen production by aromatase neurons

We hypothesized that aromatase neurons in the developing brain generate neuroestrogens from brain-born and/or circulating androgens to regulate the activity of the adjacent estrogen-sensitive cells. To test this hypothesis, we used electrophysiology on acute brain slice preparations comprising the arcuate nucleus from newborn (P4-P7) male mice with genetically labeled kisspeptin neurons. We carried out whole-cell patch-clamp experiments in current-clamp mode to record the firing of fluorescent kisspeptin neurons expressing ZsGreen. Indirect transsynaptic actions of testosterone (T) were eliminated by including picrotoxin and kynurenic acid in the aCSF. We also added the androgen receptor (AR) antagonist flutamide (100 nM) to the electrode solution to block AR-mediated direct responses of the recorded kisspeptin neuron to T. As most kisspeptin neurons showed no spontaneous activity, a 10 pA depolarizing current was applied during the entire recording period to induce and maintain firing. Firing of kisspeptin neurons (n = 33) was typically irregular with frequent burst-like patterns and 3-5 minute-long-oscillations between peaks and nadirs. This observation fitted well with the activity patterns reported for adult mice (Clarkson et al., 2017; Vanacker et al., 2017). The mean firing rate during the 5-min control period was 2.26 ± 0.54 Hz (n=7 cells) but decreased significantly following T administration (50 nM) to 54.1 ± 15.3 % of the control rate (Student's t-test, p = 0.0242) (Fig. 8 B, 1st column in Fig. 8 I and Table8-1). Neuronal activity started to decline 3.4 ± 1.1 min after T

application to the aCSF. A washout effect was reflected in the slow increase in neuronal activity 15-20 min after T treatment was suspended (Fig. 8 C). The reduced firing rate of kisspeptin neurons in response to T treatment resembled the estrogen response of adult kisspeptin neurons (Cholanian et al., 2014; Ruka et al., 2016).

This resemblance and the absence of detectable aromatase signal in kisspeptin neurons (see above) raised the possibility that T requires conversion to estradiol by aromatase neurons to inhibit kisspeptin neuron firing. Therefore, we replicated the above experiment with both T and the aromatase inhibitor letrozole (100 nM) in the aCSF. Following a 5-min control period with letrozole in the aCSF, the recording was continued for 10 min in the presence of T. Preincubation of the slice with letrozole completely prevented the effect of T on kisspeptin neuron firing (112.0 ± 8.16 % of the control value 1.8 ± 0.48 Hz, Student' t-test, p=0.2029, n=6 cells) (Fig. 8 D, 2nd column in Fig. 8 I and Table 8-1). This observation indicated that T needs to be converted to estradiol by aromatase in order to act on ERs in kisspeptin neurons. Indeed, T was unable to alter kisspeptin neuron activity in the presence of the ER inhibitor ICI182,780 (108.5 ± 16.92 % of the control value 1.8 ± 0.21 Hz, Student's t-test, p=0.632, n=8 cells) (Fig. 8 E, 3rd column in Fig. 8 I and Table 8-1). Although aromatase neurons do not seem to express kisspeptin in our immunohistochemical analyses, a recent RT/PCR study reported the presence of the aromatase transcript in pooled kisspeptin neurons of the developing murine arcuate nucleus (Alfaia et al., 2019). To rule out that T is converted to estradiol by a low level of endogenous aromatase in these cells and to prove that T acts mostly indirectly on kisspeptin neurons, letrozole (100 nM), in addition to flutamide, was added to the electrode solution and then, the effect of T re-assessed. T application in this study resulted in a significant decrease in kisspeptin neuron firing (57.7 ± 9.24 % of the control value 1.9 ± 0.31 Hz, Student's t-test, p=0.0025, n = 8 cells) (Fig. 8 F, 4th column in Fig. 8 I and Table 8-1), which was similar to the effect of T alone (1st column Fig. 8 I).

This observation indicated that endogenous aromatase has only minor, if any contribution to the T effect on kisspeptin neuron firing; therefore, the mechanism whereby T acts on kisspeptin neurons is via aromatization in other neurons. To confirm the key role of E2 in the

inhibition of arcuate kisspeptin neurons upon T administration, we replaced T with an equimolar concentration of E2 in the next experiment. Administration of 50 nM E2 evoked a substantial decrease in the firing rate of kisspeptin neurons (52.7 ± 11.47 % of the control value of 1.98 ± 0.21 Hz, Student's t-test, p=0.0091, n = 6 cells) (Fig. 8 G, 5th column in Fig. 8 I and Table 8-1), mimicking the effect of T.

If arcuate aromatase neurons account for the conversion of T to E2 in males, we hypothesized that T would not produce the same effect in females which lack aromatase neurons in the ARC. Indeed, T did not affect the firing rate of ARC kisspeptin neurons in newborn female mice (112.2 ± 8.11 % of the control value of 2.02 ± 0.19 Hz, Student's t-test, p=0.1936, n = 6 cells) (Fig. 8 H, 6th column in Fig. 8 I and Table 8-1).

The firing rates of the different treatment groups were significantly different by ANOVA (p = 0.0006) followed by Tukey's post-hoc test (T only *vs.* letrozole + T, p = 0.0379; T only *vs.* ICI182,780 + T, p = 0.0351; T only *vs.* T to female, p = 0.0369; Letrozole + T *vs.* Intraletrozole + T, p = 0.0484; letrozole + T *vs.* E2 only, p = 0.0414; ICI182,780 + T *vs.* Intraletrozole + T, p = 0.0448; ICI182,780 + T *vs.* E2 only, p = 0.0396; Intraletrozole + T *vs.* T to female, p = 0.0471; E2 only *vs.* T to female, p = 0.0404 and Table 8-2). Analysis of the control periods (before T) with ANOVA followed by Tukey's post-hoc test showed that ICI182,780 or intra/extracellular letrozole alone did not alter the firing rate (ANOVA, p = 0.9395 and Table 8-3).

DISCUSSION

To gain insight into how the maturation of the reproductive axis may be influenced by neurosteroid signaling, we used a genetic approach to analyze the development of the aromatase neuronal network in the embryonic and perinatal murine brain. Our data reveal that (1) neuronal aromatase expression, starts at E13.5 in two distinct forebrain nuclei. (2) The number of aromatase neurons increases substantially until birth but aromatase expression remains restricted to the hypothalamus and the amygdala. (3) There is no obvious major sexual dimorphism in the number and projections of aromatase neurons in the embryonic brain. (4) Most aromatase neurons do not express ERα, (5) but are in close proximity to ERα neurons, suggesting mostly local actions of neuroestrogens. (6) At birth, a cluster of aromatase neurons in the hypothalamic arcuate nucleus adjacent to kisspeptin neurons becomes apparent in males, but not in females. (7) Aromatase neurons communicate gonadal and/or brain-derived androgen signals to adjacent estrogen-sensitive neurons. Specifically, arcuate aromatase neurons in perinatal males convert testosterone to estradiol which reduces kisspeptin neuron firing via rapid actions on ERs. Taken together, our data provide a cellular substrate underlying aromatase action in the developing murine brain.

Conclusive experimental evidence documenting aromatase expression in the embryonic brain at a cellular resolution had been difficult to obtain. We found the first activity of the *Cyp19A1* promoter to be restricted to a few neurons in two distinct areas of the hypothalamus, possibly explaining the difficulties in previous experimental attempts trying to demonstrate steroid hormone production in the brain *in utero*. Aromatase expression as visualized with high sensitivity in the reporter mice is very selective and highly similar if not stereotyped in between age-matched individuals, arguing against a random stochastic activation of the promoter in this animal model. The onset of aromatase expression in the reporter mice coincides with the first ERα expression in distinct hypothalamic neurons (Kumar et al., 2014; Kumar et al., 2015) suggesting that the brain becoming estrogen-sensitive may be

orchestrated with the potential *de novo* synthesis of neurosteroids. Notably, the first aromatase-expressing cells in the entire embryo originate in the brain and not in the gonads or anywhere else. Aromatase neurons remain restricted to a few nuclei in the hypothalamus and the amygdala during embryogenesis, without obvious major differences between males and females. One caveat we need to consider is that sex differences in aromatase activity within individual aromatase neurons are not reported by the genetic labeling approach and may thus have escaped our analyses. qPCR measurements of mRNA levels did not reveal major differences between sexes. Most aromatase neurons do not express ERα during embryogenesis but are in close proximity to estrogen-sensitive cells. These data raise the possibility, that local neuroestrogen action resulting from *de novo* synthesis and/or conversion might play an active role other than sexual differentiation in the embryonic brain, for example in neural differentiation (Toran-Allerand, 1976). Consistent with this, some estradiol has indeed been detected in the embryonic rat brain using radio immune assays (Konkle and McCarthy, 2011) and estrogens were shown to promote neurite growth in the developing brain *in vitro* (Toran-Allerand et al., 1983) and in cultured fetal neurons (Carrer et al., 2005). Fetal *de novo* neurosteroid synthesis is also in line with our finding that the mRNAs of at least three key enzymes of steroid synthesis are expressed in the brain before birth. Taken together, our data demonstrate that an aromatase neuronal network consisting of well over 6000 neurons develops in both male and female embryos long before the well documented masculinizing and feminizing actions of estrogen.

The classical aromatization hypothesis states that the female brain is the default brain and that estrogen is not needed during early development (females are protected by α-fetoprotein). Accordingly, feminizing estrogen actions start postnatally, i.e. when the ovaries start to produce estradiol. Consistent with this, significant amounts of serum estrogen were not detected in female rats before P7 (Lamprecht et al., 1976). Male brains are masculinized and defeminized by estrogen aromatized from circulating testosterone originating from the testis

in later developmental stages. In contrast, our results suggest that the brain relies on estrogenic actions starting in the embryo. Because we did not detect gross sex differences in the aromatase neuronal network *in utero* in either cell numbers or mRNA expression, we propose that neuroestrogens act both in the male and female embryonic brain to establish a 'default' brain status before undergoing sexual differentiation later in development, i.e. when circulating estrogen levels rise in females or subsequent to the testosterone surge in males (Baum et al., 1991). Our data predict, that fetal neuroestrogens act mainly locally, possibly even in a paracrine manner, within distinct nuclei in the hypothalamus and the amygdala.

Aromatase and estrogen-sensitive neurons are found in close proximity, indicating that estrogen is only partially acting as a hormone but rather like a neurotransmitter. Hormones are typically released far away from their site of action and exert long lasting effects, such as changing gene expression. Neurotransmitters on the other hand act close to their release site and their effects typically occur within milliseconds (Balthazart and Ball, 2006). One prerequisite for estrogen to act as a neurotransmitter is that its synthesis and release need to be regulated within a much shorter time span than the modulation of aromatase expression levels would permit. Consistent with this, aromatase activity can be blocked by phosphorylation of two residues in the aromatase enzyme in a Ca^{2+}-dependent manner (Balthazart et al., 2001), providing a mechanism to switch off estrogen synthesis within milliseconds. In birds, aromatase was localized in axon terminals (Balthazart and Ball, 2006). We detected dense, nucleus-dependent aromatase fibers in the embryonic ArIC/eR26-τGFP brains. If aromatase is also located in the axon terminal in rodents, aromatase neurons could exert neurotransmitter-like estrogen actions far away from their cell body. Neurosteroids may act as local signaling cues, that act shortly and rapidly on neighboring cells (Kow and Pfaff, 2004; Cornil et al., 2006). We found that T reduced the firing rate of male kisspeptin neurons. One reason why kisspeptin neuron activity needs to be suppressed during the neonatal period is to silence the reproductive axis (i.e. the GnRH/ luteinizing hormone (LH) pulse generator) until puberty onset to allow proper sexual maturation. Besides its membrane effect, neuroestrogens might

568 also influence gene expression in adjacent estrogen-sensitive neurons, mediated by ERα
569 acting as a transcription factor. Future experiments will be aimed at delineating the
570 connectivity map of aromatase neurons and assign neurosteroid function to the individual
571 aromatase-expressing nuclei.
572

REFERENCES

Agulnik AI, Bishop CE, Lerner JL, Agulnik SI, Solovyev VV (1997) Analysis of mutation rates in the SMCY/SMCX genes shows that mammalian evolution is male driven. Mamm Genome 8:134-138.

Alfaia C, Robert V, Poissenot K, Levern Y, Guillaume D, Yeo S, Colledge W, Franceschini I (2019) Sexually dimorphic gene expression and neurite sensitivity to estradiol in fetal arcuate Kiss1 cells. J Endocrinol 18:e13002.

Bakker J, De Mees C, Douhard Q, Balthazart J, Gabant P, Szpirer J, Szpirer C (2006) Alpha-fetoprotein protects the developing female mouse brain from masculinization and defeminization by estrogens. Nat Neurosci 9:220-226.

Balint F, Liposits Z, Farkas I (2016) Estrogen receptor beta and 2-arachidonoylglycerol mediate the suppressive effects of estradiol on frequency of postsynaptic currents in gonadotropinreleasing hormone neurons of metestrous mice: an acute slice electrophysiological study. Front Cell Neurosci 10:77.

Balthazart J (2020) Sexual partner preference in animals and humans. Neurosci Biobehav Rev 115:34-47.

Balthazart J, Ball GF (2006) Is brain estradiol a hormone or a neurotransmitter? Trends Neurosci 29:241-249.

Balthazart J, Baillien M, Ball GF (2001) Phosphorylation processes mediate rapid changes of brain aromatase activity. J Steroid Biochem Mol Biol 79:261-277.

Balthazart J, Foidart A, Surlemont C, Harada N (1991) Distribution of aromatase-immunoreactive cells in the mouse forebrain. Cell Tissue Res 263:71-79.

Baum MJ, Woutersen PJ, Slob AK (1991) Sex difference in whole-body androgen content in rats on fetal days 18 and 19 without evidence that androgen passes from males to females. Biol Reprod 44:747-751.

Boehm U, Zou Z, Buck LB (2005) Feedback loops link odor and pheromone signaling with reproduction. Cell 123:683-695.

600 Candlish M, Wartenberg P, Boehm U (2018) Genetic strategies examining kisspeptin
601 regulation of GnRH neurons. In: The GnRH neuron and its control (Allan H, ed), pp259-287.
602 Hoboken: Wiley Blackwell.
603 Carrer HF, Cambiasso MJ, Gorosito S (2005) Effects of estrogen on neuronal growth and
604 differentiation. J Steroid Biochem Mol Biol 93:319-323.
605 Cholanian M, Krajewski-Hall SJ, Levine RB, McMullen NT, Rance NE (2014)
606 Electrophysiology of arcuate neurokinin B neurons in female Tac2-EGFP transgenic mice.
607 Endocrinology 155:2555-2565.
608 Chu Z, Andrade J, Shupnik MA, Moenter SM (2009) Differential regulation of gonadotropin-
609 releasing hormone neuron activity and membrane properties by acutely applied estradiol:
610 dependence on dose and estrogen receptor subtype. J Neurosci 29, 5616–5627.
611 Clarkson J, Han SY, Piet R, McLennan T, Kane GM, Ng J, Porteous RW, Kim JS, Colledge
612 WH, Iremonger KJ, Herbison AE (2017) Definition of the hypothalamic GnRH pulse
613 generator in mice. Proc Natl Acad Sci USA 114:E10216-E10223.
614 Cornil CA, Taziaux M, Baillien M, Ball GF, Balthazart J (2006) Rapid effects of aromatase
615 inhibition on male reproductive behaviors in Japanese quail. Horm Behav 49:45-67.
616 De Mees C, Bakker J, Szpirer J, Szpirer C (2007) Alpha-fetoprotein: from a diagnostic
617 biomarker to a key role in female fertility. Biomark Insights 1:82-85.
618 Dubois SL, Wolfe A, Radovick S, Boehm U, Levine JE (2016) Estradiol restrains prepubertal
619 gonadotropin secretion in female mice via activation of ERalpha in kisspeptin neurons.
620 Endocrinology 157:1546-1554.
621 Dubois SL, Acosta-Martinez M, DeJoseph MR, Wolfe A, Radovick S, Boehm U, Urban JH,
622 Levine JE (2015) Positive, but not negative feedback actions of estradiol in adult female mice
623 require estrogen receptor alpha in kisspeptin neurons. Endocrinology 156:1111-1120.
624 Glanowska KM, Venton BJ, Moenter SM (2012) Fast scan cyclic voltammetry as a novel
625 method for detection of real-time gonadotropin-releasing hormone release in mouse brain
626 slices. J Neurosci 32:14664-14669.

627 Kapourchali FR, Louis XL, Eskin MNA, Suh M (2020) A pilot study on the effect of early
628 provision of dietary docosahexaenoic acid on testis development, functions, and sperm quality
629 in rats exposed to prenatal ethanol. Birth Defects Res 112:93-104.
630 Kenealy BP, Keen KL, Garcia JP, Kohlenberg LK, Terasawa E (2017) Obligatory role of
631 hypothalamic neuroestradiol during the estrogen-induced LH surge in female ovariectomized
632 rhesus monkeys. Proc Natl Acad Sci USA 114:13804-13809.
633 Kenealy BP, Kapoor A, Guerriero KA, Keen KL, Garcia JP, Kurian JR, Ziegler TE, Terasawa
634 E (2013) Neuroestradiol in the hypothalamus contributes to the regulation of gonadotropin
635 releasing hormone release. J Neurosci 33:19051-19059.
636 Konkle AT, McCarthy MM (2011) Developmental time course of estradiol, testosterone, and
637 dihydrotestosterone levels in discrete regions of male and female rat brain. Endocrinology
638 152:223-235.
639 Kow LM, Pfaff DW (2004) The membrane actions of estrogens can potentiate their lordosis
640 behavior-facilitating genomic actions. Proc Natl Acad Sci USA 101:12354-12357.
641 Kretz O, Fester L, Wehrenberg U, Zhou L, Brauckmann S, Zhao S, Prange-Kiel J, Naumann
642 T, Jarry H, Frotscher M, Rune GM (2004) Hippocampal synapses depend on hippocampal
643 estrogen synthesis. J Neurosci 24:5913-5921.
644 Kumar D, Boehm U (2014) Conditional genetic transsynaptic tracing in the embryonic mouse
645 brain. J Vis Exp 94:52487.
646 Kumar D, Periasamy V, Freese M, Voigt A, Boehm U (2015) In Utero Development of
647 Kisspeptin/GnRH Neural Circuitry in Male Mice. Endocrinology 156:3084-3090.
648 Kumar D, Freese M, Drexler D, Hermans-Borgmeyer I, Marquardt A, Boehm U (2014)
649 Murine arcuate nucleus kisspeptin neurons communicate with GnRH neurons in utero. J
650 Neurosci 34:3756-3766.
651 Lamprecht SA, Kohen F, Ausher J, Zor U, Lindner HR (1976) Hormonal stimulation of
652 oestradiol-17 beta release from the rat ovary during early postnatal development. J Endocrinol
653 68:343-344.

654 Lauber ME, Lichtensteiger W (1994) Pre- and postnatal ontogeny of aromatase cytochrome
655 P450 messenger ribonucleic acid expression in the male rat brain studied by in situ
656 hybridization. Endocrinology 135:1661-1668.
657 Lehman MN, Coolen LM, Goodman RL (2010) Minireview: kisspeptin/neurokinin
658 B/dynorphin (KNDy) cells of the arcuate nucleus: a central node in the control of
659 gonadotropin-releasing hormone secretion. Endocrinology 151:3479-3489.
660 Lephart ED, Simpson ER, McPhaul MJ, Kilgore MW, Wilson JD, Ojeda SR (1992) Brain
661 aromatase cytochrome P-450 messenger RNA levels and enzyme activity during prenatal and
662 perinatal development in the rat. Brain Res Mol Brain Res 16:187-192.
663 Mayer C, Acosta-Martinez M, Dubois SL, Wolfe A, Radovick S, Boehm U, Levine JE (2010)
664 Timing and completion of puberty in female mice depend on estrogen receptor alpha-
665 signaling in kisspeptin neurons. Proc Natl Acad Sci USA 107:22693-22698.
666 McCarthy MM (2008) Estradiol and the developing brain. Physiol rev 88:91-124.
667 Micevych PE, Meisel RL (2017) Integrating neural circuits controlling female sexual
668 behavior. Front Syst Neurosci 11:42.
669 Mombaerts P, Wang F, Dulac C, Chao SK, Nemes A, Mendelsohn M, Edmondson J, Axel R
670 (1996) Visualizing an olfactory sensory map. Cell 87:675-686.
671 Paxinos G, Halliday GM, Watson C, Koutcherov Y, Wang H (2007) Atlas of the Developing
672 Mouse Brain. Cambridge, MA: Elsevier Inc.
673 Pielecka-Fortuna J, Chu Z, Moenter SM (2008) Kisspeptin acts directly and indirectly to
674 increase gonadotropin-releasing hormone neuron activity and its effects are modulated by
675 estradiol. Endocrinology 149:1979-1986.
676 Ruka KA, Burger LL, Moenter SM (2016) Both estrogen and androgen modify the response
677 to activation of neurokinin-3 and kappa-opioid receptors in arcuate kisspeptin neurons from
678 male mice. Endocrinology 157:752-763.
679 Sanghera MK, Simpson ER, McPhaul MJ, Kozlowski G, Conley AJ, Lephart ED (1991)
680 Immunocytochemical distribution of aromatase cytochrome P450 in the rat brain using
681 peptide-generated polyclonal antibodies. Endocrinology 129:2834-2844.

682 Santen RJ, Brodie H, Simpson ER, Siiteri PK, Brodie A (2009) History of aromatase: saga of
683 an important biological mediator and therapeutic target. Endocr Rev 30:343-375.
684 Sasano H, Takashashi K, Satoh F, Nagura H, Harada N (1998) Aromatase in the human
685 central nervous system. Clin Endocrinol (Oxf) 48:325-329.
686 Scarduzio M, Panichi R, Pettorossi VE, Grassi S (2013) Synaptic long-term potentiation and
687 depression in the rat medial vestibular nuclei depend on neural activation of estrogenic and
688 androgenic signals. PloS One 8:e80792.
689 Schambra U (2008) Prenatal Mouse Brain Atlas, New York, NY: Springer US.
690 Scordalakes EM, Rissman EF (2004) Aggression and arginine vasopressin immunoreactivity
691 regulation by androgen receptor and estrogen receptor alpha. Genes Brain Behav 3:20-26.
692 Stanic D, Dubois S, Chua HK, Tonge B, Rinehart N, Horne MK, Boon WC (2014)
693 Characterization of aromatase expression in the adult male and female mouse brain. I.
694 Coexistence with oestrogen receptors alpha and beta, and androgen receptors. PloS One
695 9:e90451.
696 Toran-Allerand CD (1976) Sex steroids and the development of the newborn mouse
697 hypothalamus and preoptic area in vitro: implications for sexual differentiation. Brain Res
698 106:407-412.
699 Toran-Allerand CD (2005) Estrogen and the brain: beyond ER-alpha, ER-beta, and 17beta-
700 estradiol. Ann N Y Acad Sci 1052:136-144.
701 Toran-Allerand CD, Hashimoto K, Greenough WT, Saltarelli M (1983) Sex steroids and the
702 development of the newborn mouse hypothalamus and preoptic area in vitro: III. Effects of
703 estrogen on dendritic differentiation. Brain Res 283:97-101.
704 Travison TG, Vesper HW, Orwoll E, Wu F, Kaufman JM, Wang Y, Lapauw B, Fiers T,
705 Matsumoto AM, Bhasin S (2017) Harmonized reference ranges for circulating testosterone
706 levels in men of four cohort studies in the United States and Europe. J Clin Endocrinol Metab
707 102:1161-1173.
708 Unger EK, Burke KJ, Jr., Yang CF, Bender KJ, Fuller PM, Shah NM (2015) Medial
709 amygdalar aromatase neurons regulate aggression in both sexes. Cell Rep 10:453-462.

710 Vanacker C, Moya MR, DeFazio RA, Johnson ML, Moenter SM (2017) Long-Term
711 recordings of arcuate nucleus kisspeptin neurons reveal patterned activity that is modulated
712 by gonadal steroids in male mice. Endocrinology 158:3553-3564.
713 Ventura-Aquino E, Paredes RG (2020) Sexual behavior in rodents: Where do we go from
714 here? Horm Behav 118:104678.
715 Vreeburg JT, van der Vaart PD, van der Schoot P (1977) Prevention of central defeminization
716 but not masculinization in male rats by inhibition neonatally of oestrogen biosynthesis. J
717 Endocrinol 74:375-382.
718 Wacker DW, Khalaj S, Jones LJ, Champion TL, Davis JE, Meddle SL, Wingfield JC (2016)
719 Dehydroepiandrosterone heightens aggression and increases androgen receptor and aromatase
720 mRNA expression in the brain of a male songbird. J Neuroendocrinol 28:12443.
721 Wagner CK, Morrell JI (1997) Neuroanatomical distribution of aromatase MRNA in the rat
722 brain: indications of regional regulation. J Steroid Biochem Mol Biol 61:307-314.
723 Walker VR, Korach KS (2004) Estrogen receptor knockout mice as a model for endocrine
724 research. ILAR J 45:455-461.
725 Wang L, Burger LL, Greenwald-Yarnell ML, Myers MG, Jr., Moenter SM (2018)
726 Glutamatergic transmission to hypothalamic kisspeptin neurons is differentially regulated by
727 estradiol through estrogen receptor alpha in adult female mice. J Neurosci 38:1061-1072.
728 Wen S, Gotze IN, Mai O, Schauer C, Leinders-Zufall T, Boehm U (2011) Genetic
729 identification of GnRH receptor neurons: a new model for studying neural circuits underlying
730 reproductive physiology in the mouse brain. Endocrinology 152:1515-1526.
731 Wu MV, Manoli DS, Fraser EJ, Coats JK, Tollkuhn J, Honda S, Harada N, Shah NM (2009)
732 Estrogen masculinizes neural pathways and sex-specific behaviors. Cell 139:61-72.
733 Yang Y, Fang Z, Dai Y, Wang Y, Liang Y, Zhong X, Wang Q, Hu Y, Zhang Z, Wu D, Xu X
734 (2018) Bisphenol-A antagonizes the rapidly modulating effect of DHT on spinogenesis and
735 long-term potentiation of hippocampal neurons. Chemosphere 195:567-575.

736 Yeo SH, Kyle V, Morris PG, Jackman S, Sinnett-Smith LC, Schacker M, Chen C, Colledge
737 WH (2016) Visualisation of Kiss1 neurone distribution using a Kiss1-CRE transgenic mouse.
738 J Neuroendocrinol 28:12435.
739 Yip SH, Boehm U, Herbison AE, Campbell RE (2015) Conditional viral tract tracing
740 delineates the projections of the distinct kisspeptin neuron populations to gonadotropin-
741 releasing hormone (GnRH) neurons in the mouse. Endocrinology 156:2582-2594.
742

743 **FIGURE LEGENDS**

744

745 **Figure 1:** Genetic analysis of aromatase expression in mouse embryos. A, Aromatase and
746 τGFP reporter expression are genetically coupled in Aromatase-IRES-Cre/enhanced
747 ROSA26-τGFP (ArIC/eR26-τGFP) mice, providing a fluorescent readout for *Cyp19a1*
748 promotor activity. B, Quantification of aromatase neurons during embryonic development
749 (E13.5 *vs.* E16.5 unpaired Student's T-tests: $p < 0.0001$; E16.5 male *vs.* E18.5 female
750 unpaired Student's T-tests: $p = 0.0127$, E16.5 *vs.* E18.5 female unpaired Student's T-tests: $p =$
751 0.0035). Detailed cell counts for each nucleus are reported in Table 1-1, 1-2 and 1-3. C-D,
752 Reporter expression in the medial preoptic area at embryonic days (E) 12,5, 13.5, 16.5 and
753 18.5. E-F, Numerous contacts between aromatase perikarya (unfilled arrowheads) and fibers
754 (filled arrowheads) as shown in the amygdala, the medial preoptic area (MPOA) and
755 dorsomedial nucleus (DM). Scale bars, C and D 100 μm, E and F 25 μm. 3V, third ventricle;
756 LV, lateral ventricle.

757

758 **Figure 2:** Aromatase expression at embryonic day (E) 18.5. A, Schematic sagittal overview
759 (Schambra, 2008). Reporter gene expression is restricted to green-labeled areas. Grey insets
760 show – from lateral to medial – additional schematic sagittal overviews. B, Aromatase
761 expression in the amygdala close to the lateral ventricle. Immunofluorescent analyses
762 showing reporter gene expression (green) and nuclear staining (Hoechst 33258, blue). C,
763 Magnified image of the area indicated in B. White arrowheads indicate labeled somata in
764 close contact with labeled fibers in this nucleus. D-E, Magnified images of the areas indicated
765 in A (grey insets). Aromatase expression in the *stria terminalis* (D) and in the hypothalamus
766 (E). Scalebars: B, D and E: 500 μm, C: 50 μm. 3V, third ventricle.

767

768 **Figure 3**: qPCR analyses for *Cyp11a1*, *Cyp17a1* and *Cyp19a1* mRNAs in the brain of E12.5,
769 E13.5, E16.5 and E18.5 embryos. Note the barely detectable *Cyp19a1* mRNA at E12.5.
770 Except for *Cyp17a1* expression at E13.5, no sexual dimorphism was detected.
771
772 **Figure 4:** Estrogen-sensitive neural circuits *in utero*. A, Double immunofluorescence for
773 ERα (red) and τGFP (green) of sagittal sections through the medial preoptic area (MPOA) of
774 male and female ArIC/eR26-τGFP embryos at different ages. Note that most male aromatase
775 neurons do not express ERα. Nuclear counterstain (Hoechst 33258, blue). Arrowheads mark
776 aromatase (unfilled), ERα (dotted unfilled) and double-positive neurons (filled), respectively.
777 Scalebars: 250 μm (overviews), 50 μm (details). 3V, third ventricle; LV, lateral ventricle;
778 MPN, median preoptic nucleus. B, Quantification of ERα expression in aromatase neurons in
779 male and female embryos. Detailed double-positive cell numbers and ratios for each nucleus
780 are reported in Table 4-1, 4-2 and 4-3.
781
782 **Figure 5:** Close proximity of aromatase neurons to estrogen-sensitive circuits. Double
783 immunofluorescence for ERα (red) and τGFP (green) of sagittal sections through the medial
784 preoptic area (MPOA) of male and female ArIC/eR26-τGFP embryos at different ages.
785 Graphs show the distance between aromatase and ERα neurons. Scalebars: 100 μm. 3V, third
786 ventricle; LV, lateral ventricle.
787
788 **Figure 6:** Summary of reporter gene expression in the P0 brain. Schematic coronal
789 representations taken from (Paxinos et al., 2007). Distances (in mm) from the most rostral
790 section of the atlas are indicated. Green circles and triangles indicate areas with similar
791 numbers of cell bodies and fibers in males and females. Blue symbols indicate areas with
792 more cell bodies and fibers in males. Pink symbols indicate areas with more cell bodies and
793 fibers in females. No reporter gene expression was detected in more rostral or caudal sections.
794 Detailed cell number counts are presented in Extended Data Table 6-1 and 6-2.

Figure 7: Aromatase and kisspeptin expression in distinct nuclei of the hypothalamus and amygdala at E18.5. A, Schematic sagittal overview of the regions shown in B-G. Arc, arcuate nucleus; DM, dorsomedial nucleus; MPOA, medial preoptic area. B-G, Double immunofluorescence for kisspeptin (red) and τGFP (green). Note that aromatase is not expressed in the embryonic Arc (Fig. 7-1, Fig. 7-2) (delineated by kisspeptin labeling (Kumar et al., 2014)). 3V, third ventricle. B, Sagittal section through the hypothalamus of a male embryo at E18.5. C, Reporter expression in the MPOA. D, Arc. E-G, Aromatase and kisspeptin expression in females. Scale bars, (B-F) 250 μm (overview), 50 μm (inset). Schematic reference picture taken from (Schambra, 2008).

Figure 8: Sexually dimorphic aromatase expression in the arcuate nucleus (Arc) and direct actions of testosterone (T) on kisspeptin neuron firing. A, Reporter gene expression was only detected in the male Arc after birth. Arcuate aromatase is not expressed in kisspeptin neurons. Arrowheads indicate kisspeptin (filled) and aromatase (unfilled) neurons, respectively. 3V, third ventricle. B-H Representative traces recorded from kisspeptin neurons in the male (B-G) and female (H) Arc. B, Decreased firing rate in response to T administration. C, The effect of T could be washed out slowly. D, Presence of letrozole in the extracellular solution prevented the action of T. E, The ER-antagonist ICI182,780 also abolished the action of T. F, Intracellular administration of letrozole showed no antagonistic effect, unlike its extracellular use in D. G, Mimicking the effect of T, 17β-estradiol (E2) reduced arcuate kisspeptin neuron firing in males. H, T had no effect on the firing of kisspeptin neurons in females, which lack arcuate aromatase neurons. For experimental details, see main text. I, Testosterone (T) reduced kisspeptin neuron firing in males only. This action was entirely prevented by prior bath application of the aromatase inhibitor letrozole or the ER-inhibitor ICI182780, indicating that T conversion to E2 and ERs play a role in the effect of T. Estradiol was not derived from the recorded kisspeptin neurons, because letrozole in the electrode solution (Intraletrozole) did not interfere with T actions. T only, $p = 0.0242$; Intraletrozole + T, $p = 0.0025$; E2 only, p

823 = 0.0091 by Student's t tests. For detailed statistics see Table 8-1, 8-2 and 8-3. Scalebars: 50
824 μm.
825
826 Figure 9: Model of estrogenic actions on kisspeptin neurons in the male arcuate nucleus.
827 Testosterone, either of gonadal or neuronal origin, is converted by arcuate aromatase neurons
828 to E2 and acts on membrane-bound estrogen receptor α (ERα) in adjacent kisspeptin neurons
829 reducing their neuronal firing rate. Both T and E2 could also exert genomic effects via
830 nuclear androgen receptor (AR) and ERα in kisspeptin neurons. Because a small subset of
831 aromatase neurons expresses ERα, E2 could also exert genomic effects in these cells.
832

833 **TABLE LEGENDS**

834 **Table 1:** Aromatase neuron distribution in the developing mouse brain, + for cell bodies (+: 0
835 - 100, ++: 100 – 500, +++: 500 – 1500, ++++: 1500 – 10000), * for fibers (*: sparse, **:
836 moderate, ***: dense, ****: very dense). Abbreviations: AHiAL: amygdalohippocampal area,
837 bnst: bed nucleus of stria terminalis, Co: cortical amygdaloid nucleus, DM: dorsomedial
838 nucleus, LH: lateral hypothalamic area, LPO: lateral preoptic area, Me: medial amygdaloid
839 nucleus, MPOA: medial preoptic area, MTu: medial tuberal nucleus, opt: optic tract, PVN:
840 paraventricular nucleus, st: stria terminalis, VM: ventromedial nucleus.
841

EXTENDED DATA LEGENDS

Figure 7-1: In the E13.5 hypothalamus, ERα immunoreactivity (red, filled arrowheads) was found in the MPOA close to τGFP signal (green, unfilled arrowheads). Note that reporter gene expression (green) was not detected in the arcuate nucleus (Arc). Nuclear stain (Hoechst 33258, blue). Scalebar: 50 μm. LV, lateral ventricle.

Figure 7-2: Kisspeptin immunoreactivity (red) in the arcuate nucleus (Arc) at E16.5. Note the absence of reporter gene expression (green) in the Arc. 3V, third ventricle; DM, dorsomedial nucleus; OE, olfactory epithelium; LV, lateral ventricle; MPOA, medial preoptic area. Nuclear stain (Hoechst 33258, blue). Scalebar: 100 μm.

Table 1-1: Summary of τGFP expression in E13.5 brains. + for fibers (+: sparse, ++: moderate, +++: dense, ++++: very dense).

Table 1-2: Summary of τGFP expression in E16.5 brains. + for fibers (+: sparse, ++: moderate, +++: dense, ++++: very dense). Significant p-values indicated as asterisk next to the nucleus name. * = 0.0258.

Table 1-3: Summary of τGFP expression in E18.5 brains. + for fibers (+: sparse, ++: moderate, +++: dense, ++++: very dense). Significant p-values indicated as asterisk next to the nucleus name. * = 0.0344.

Table 4-1: Summary of colocalization between τGFP and ERα in percentage in E13.5 brains. Total double-positive cell number is represented as + (-: 0, +: 1-10, ++: 11-50, 51-100: +++, >100: ++++).

868

869 **Table 4-2:** Summary of colocalization between τGFP and ERα in percentage in E16.5 brains.
870 Total double-positive cell number is represented as + (-: 0, +: 1-10, ++: 11-50, 51-100: +++,
871 >100: ++++).

872

873 **Table 4-3:** Summary of colocalization between τGFP and ERα in percentage in E18.5 brains.
874 Total double-positive number is represented as + (-: 0, +: 1-10, ++: 11-50, 51-100: +++,
875 >100: ++++). Significant p-values indicated as asterisk next to the nucleus name.

876

877 **Table 6-1:** Summary of τGFP expression in P0 brains. + for fibers (+: sparse, ++: moderate,
878 +++: dense, ++++: very dense). Significant p-values indicated as asterisk next to the nucleus
879 name. * = 0.0418.

880

881 **Table 6-2:** Summary of colocalization between τGFP and ERα in percentage in P0 brains.
882 Total double-positive cell number is represented as + (-: 0, +: 1-10, ++: 11-50, 51-100: +++,
883 >100: ++++). Significant p-values indicated as asterisk next to the nucleus name. ** =
884 0.0018., * = 0.0218 (medial amygdaloid nucleus, posterodorsal part); * = 0.0390
885 (posteromedial cortical amygdaloid nucleus).

886

887 **Table 8-1:** Statistical analysis of changes in the firing rate of kisspeptin neurons in response
888 to T and E2 (Student's t-tests). N=number of neurons measured. n=number of animals used
889 for a given experiment. df=degree of freedom in Student's t-test of percentage changes, with
890 each neuron serving as its own control. t="t" values of Student's t-test of percentage changes.
891 p="p" probability values of Student's t-test of percentage changes. *=significant change.

T=Testosterone; letrozole=aromatase inhibitor; ICI182,780=estrogen receptor antagonist; Intraletrozole=intracellularly applied letrozole; E2=17β-estradiol.

Table 8-2: ANOVA+Tukey's post-hoc analysis to compare firing rates in the "T only", "letrozole + T", "ICI182,780 + T", "Intraletrozole + T", "E2" and "T to female" treatment groups. df=degree of freedom of ANOVA-test of percentage data. F="F" values of ANOVA-test of percentage data. p="p" probability values of ANOVA or Tukey's post-hoc test of percentage data. *=significant difference. T=Testosterone; letrozole=aromatase inhibitor; ICI182,780=estrogen receptor antagonist; Intraletrozole=intracellularly applied letrozole; E2=17β-estradiol.

Table 8-3: ANOVA analysis of the firing rates during the control periods (before T administration or E2), to compare the "T only", "letrozole + T", "ICI182,780 + T", "Intraletrozole + T", "E2 only" and "T to female" treatment groups. T=Testosterone; letrozole=aromatase inhibitor; ICI182,780=estrogen receptor antagonist; Intraletrozole=intracellularly applied letrozole; E2=17β-estradiol

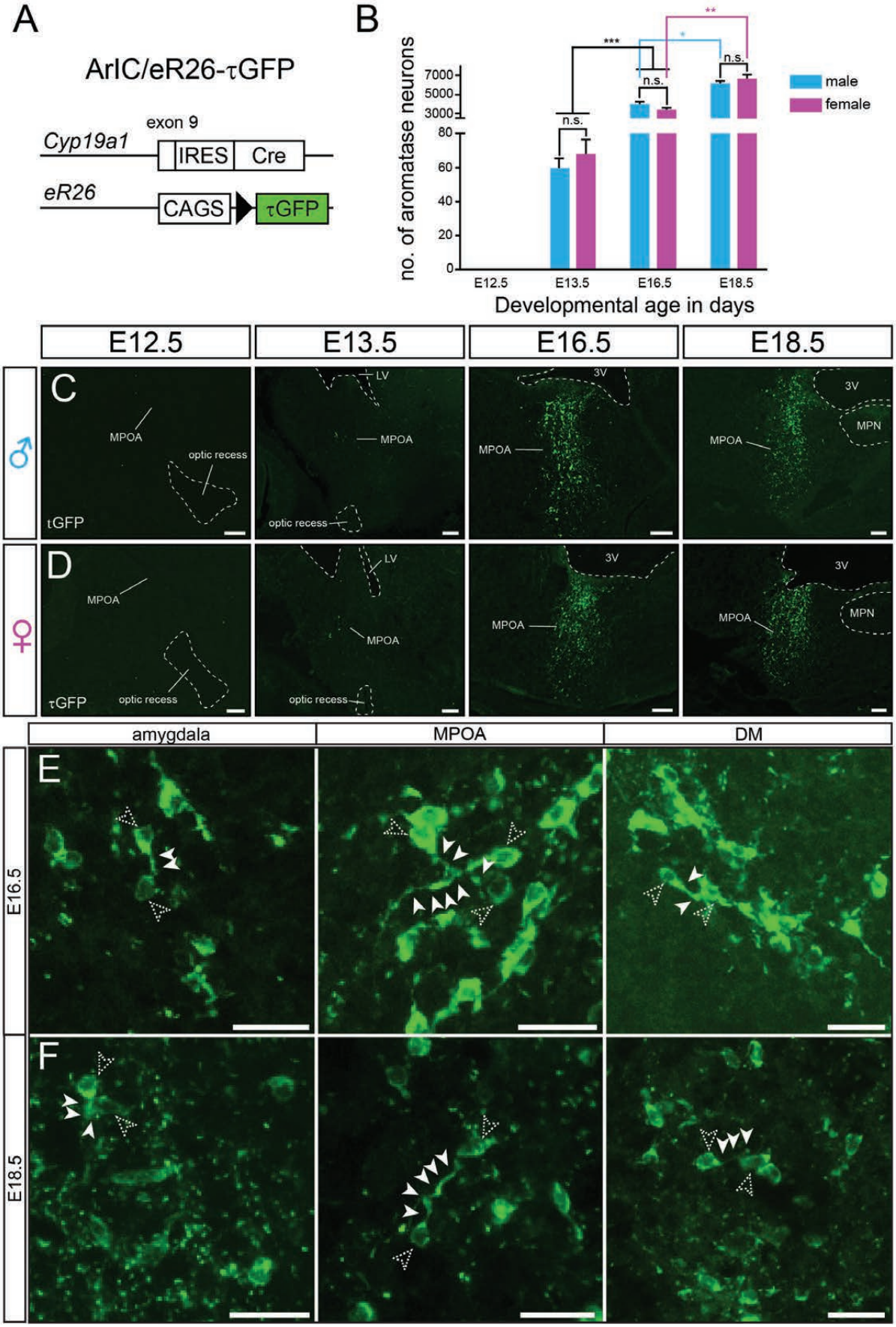

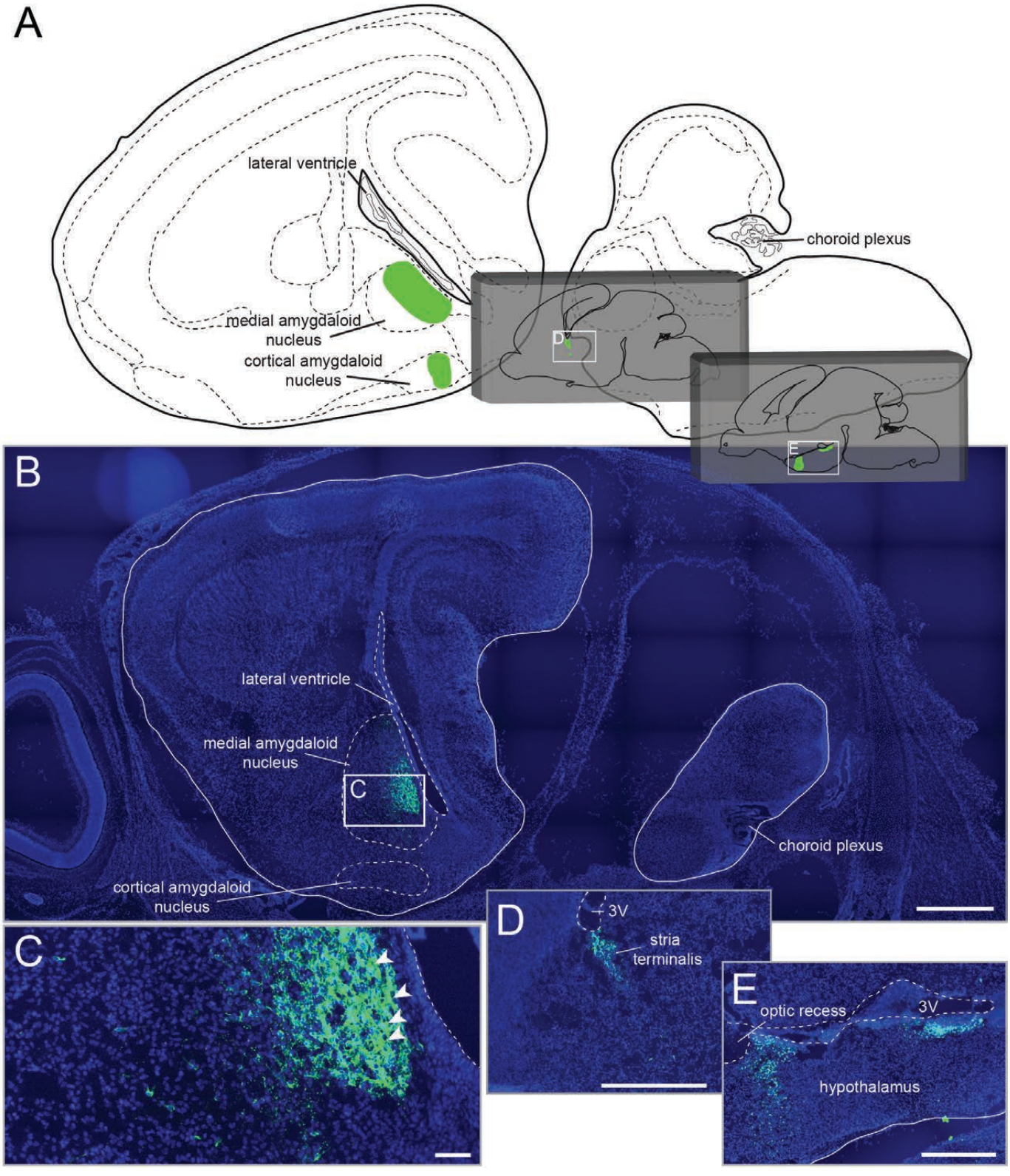

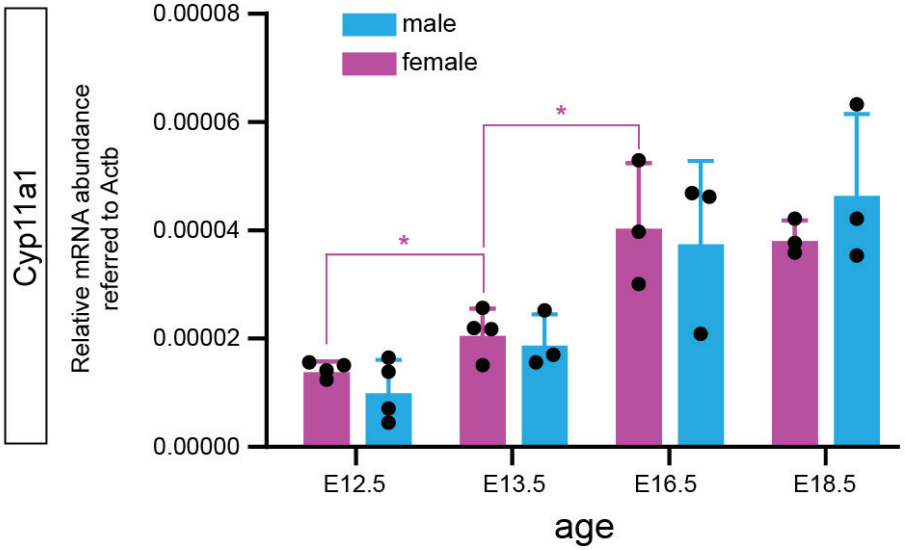

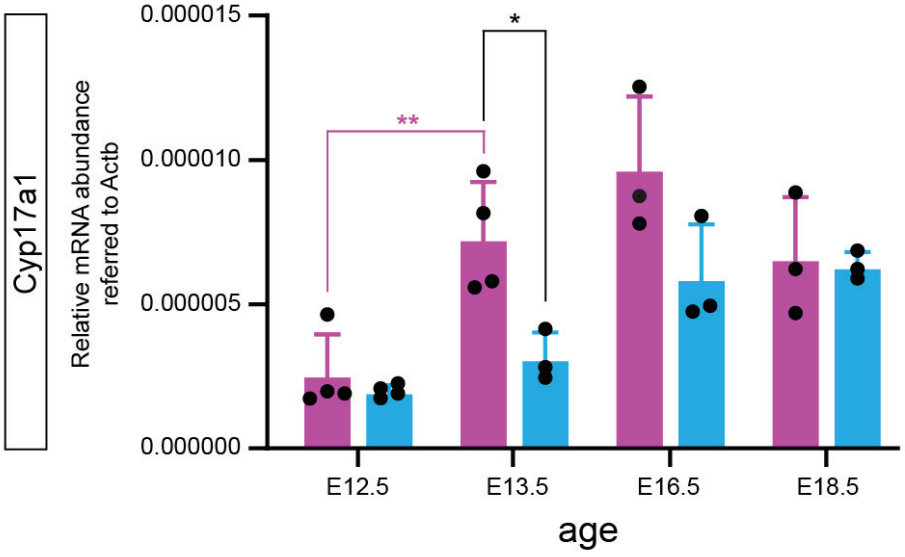

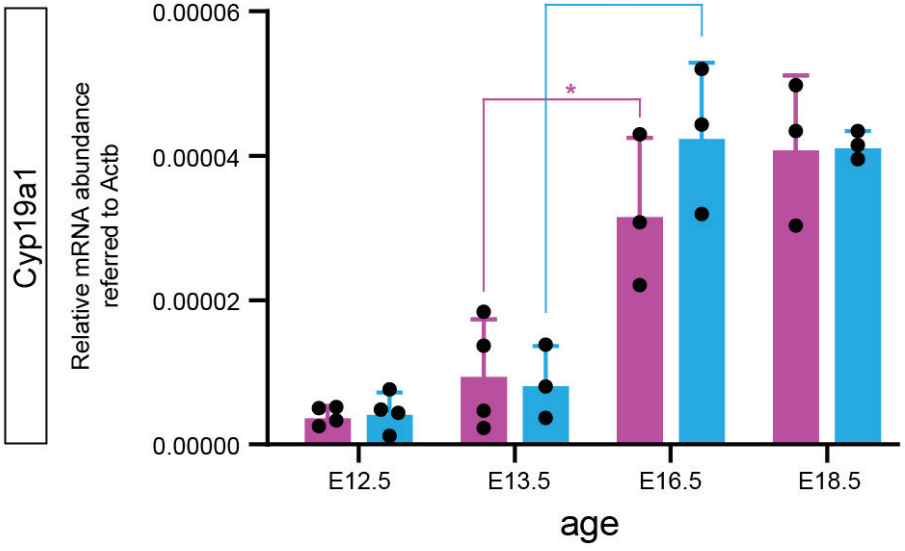

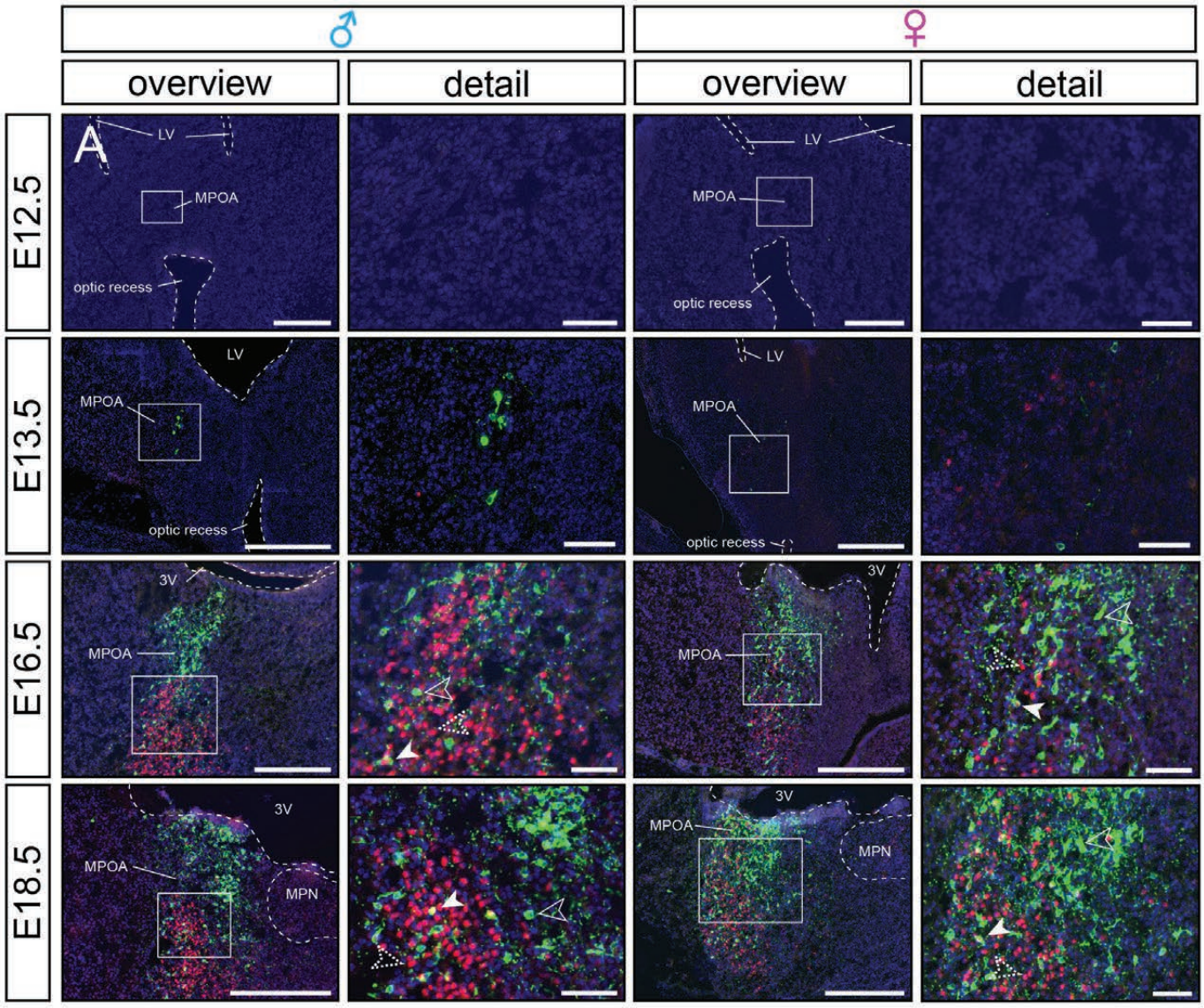

B

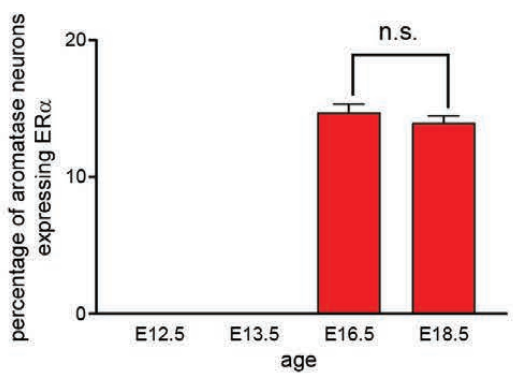

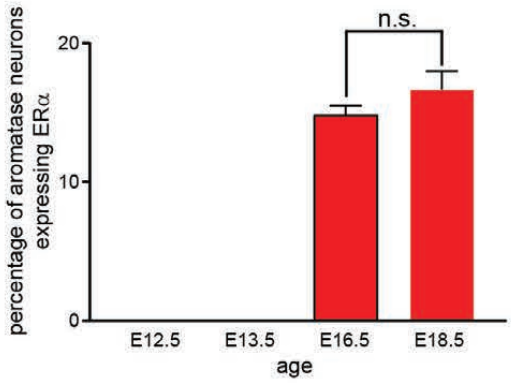

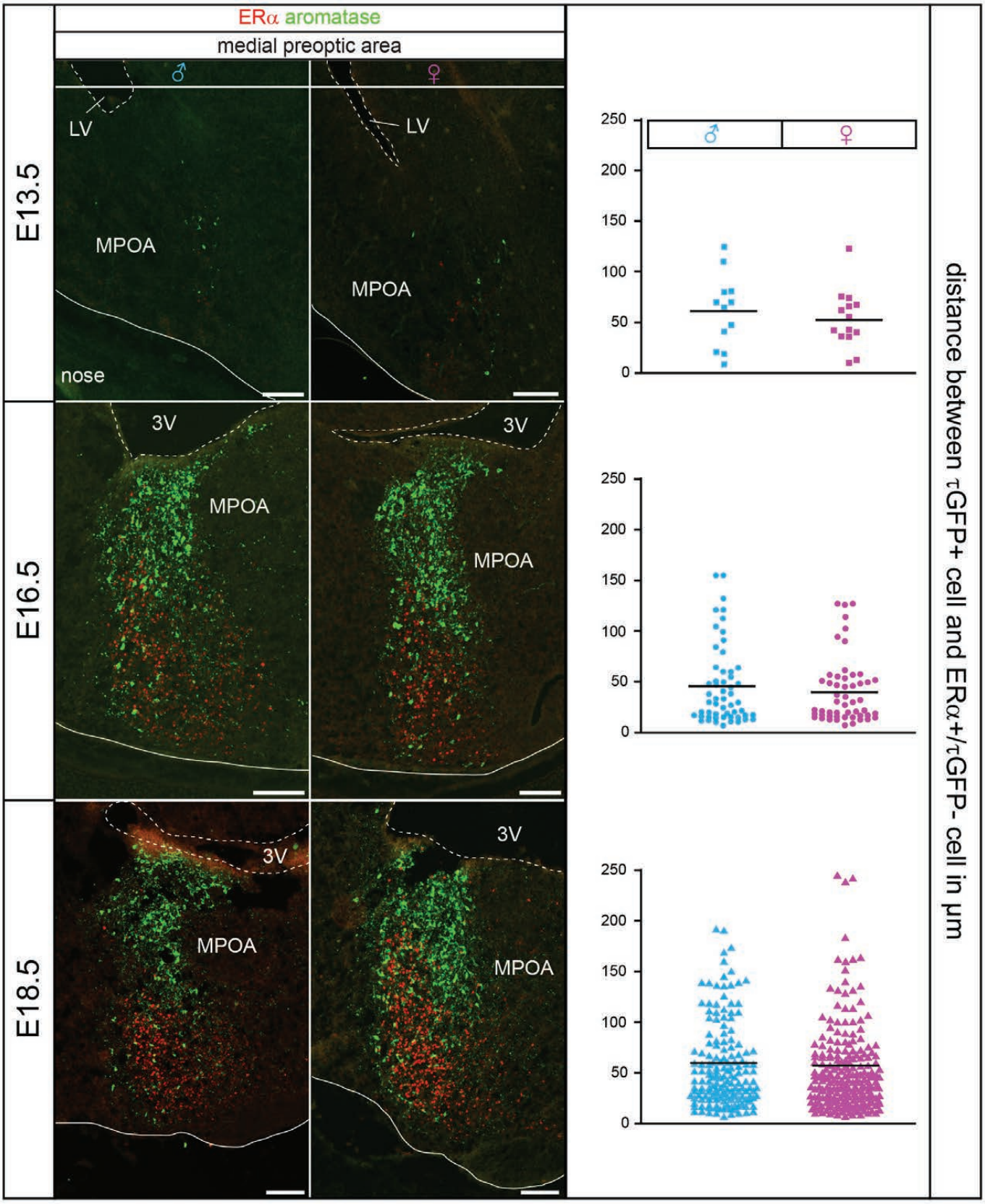

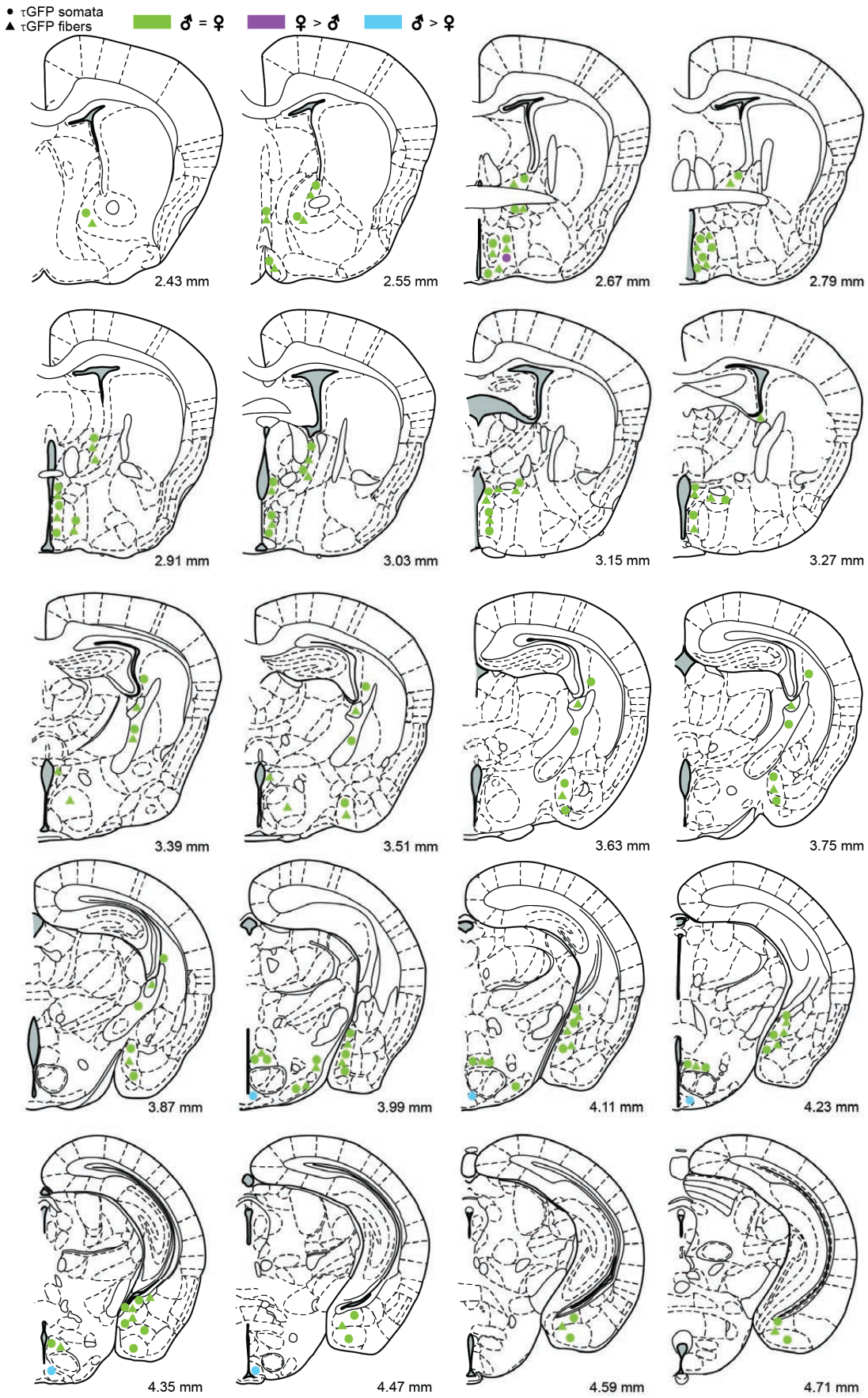

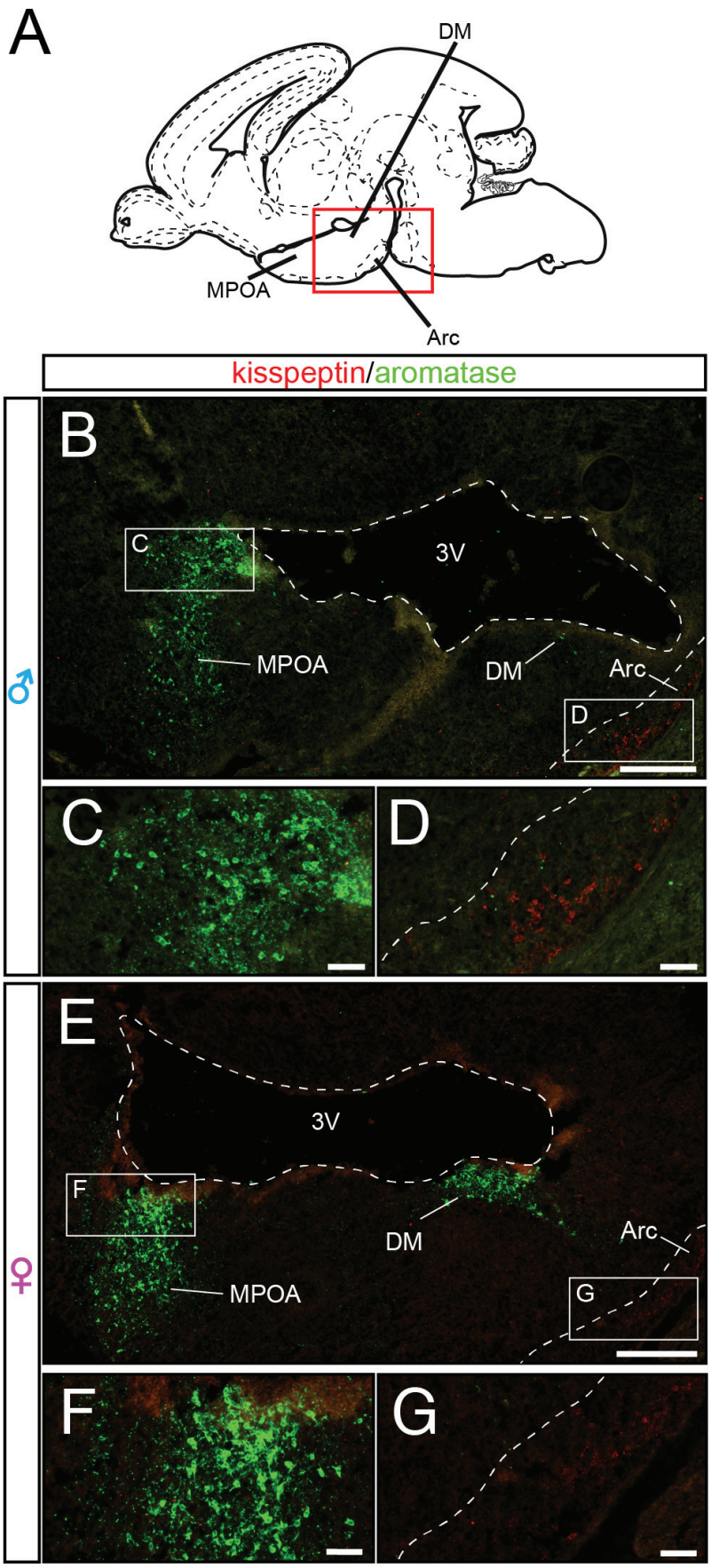

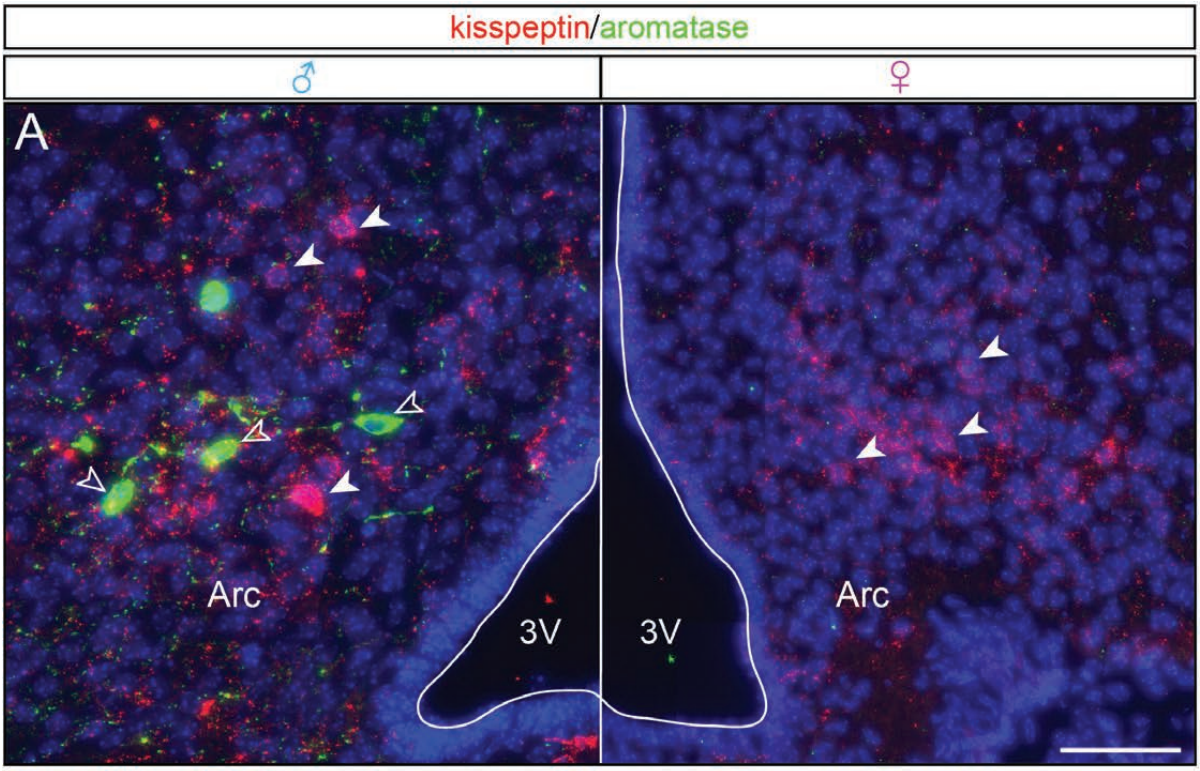

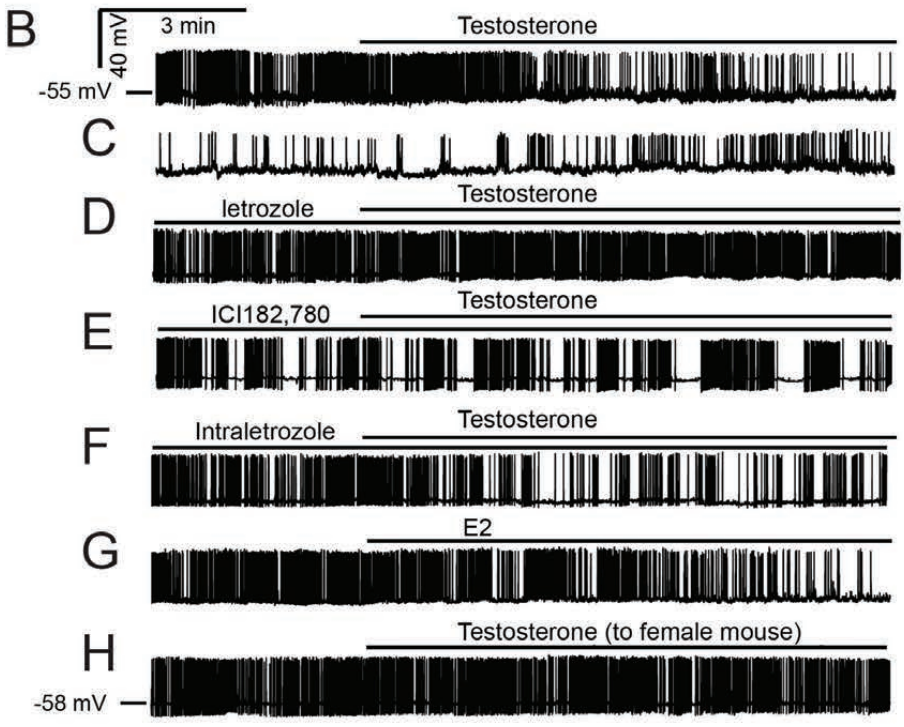

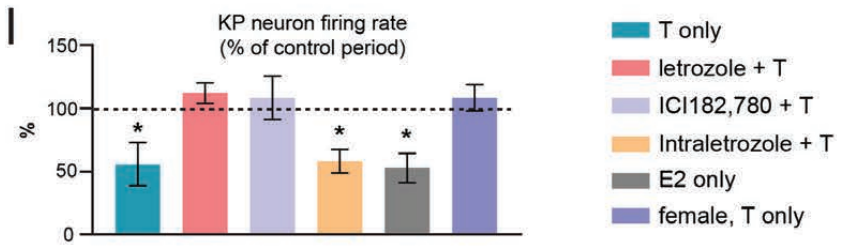

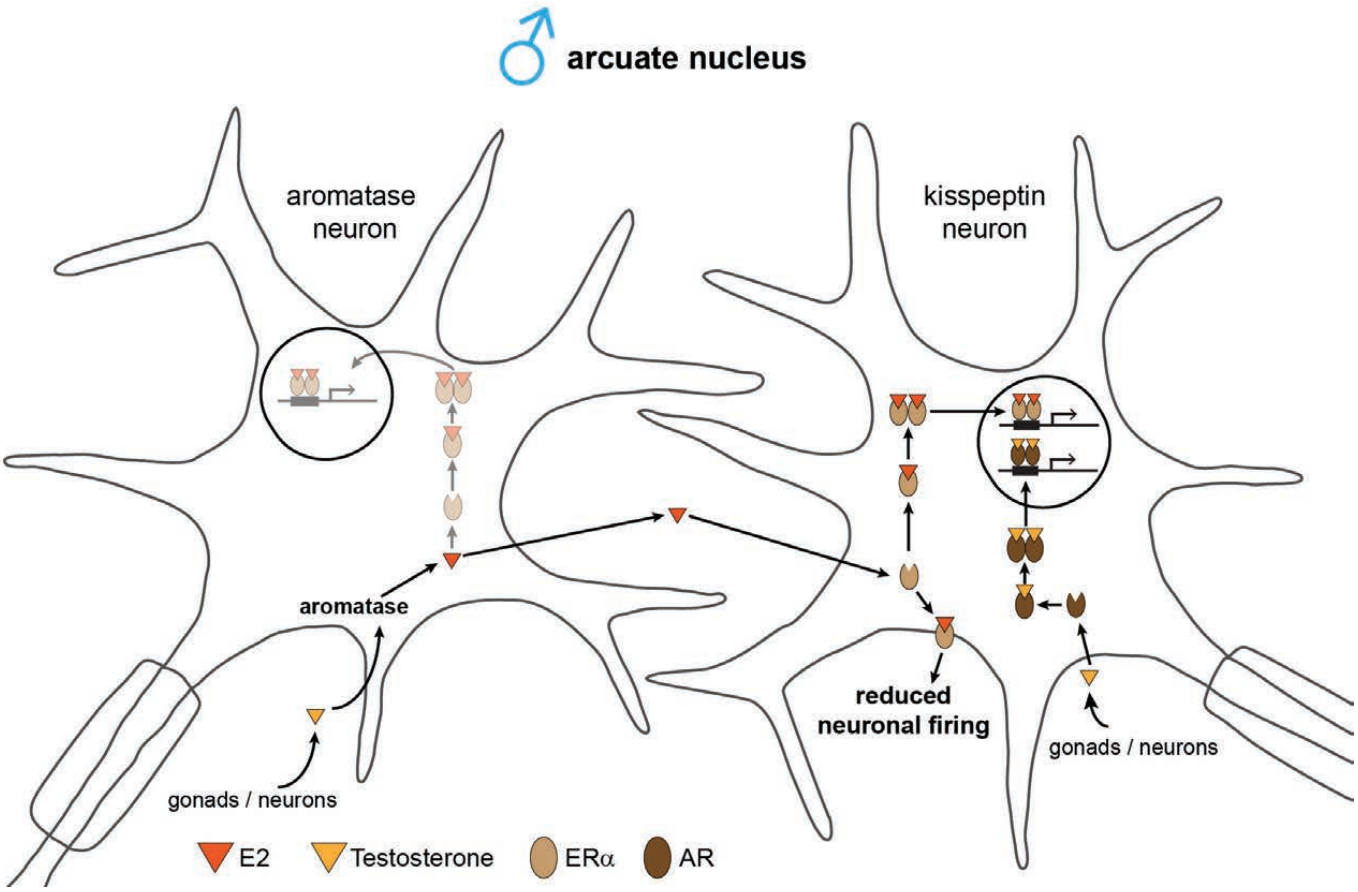

Table 1

		E13.5		E16.5		E18.5	
	Structure	♂	♀	♂	♀	♂	♀
Amygdala	AhiAL	- -	- -	- -	- -	++ *	++ *
	Co	- -	- -	++ *	++ *	++ **	+ **
	Me	- -	- -	+++ ****	+++ ****	+++ ****	+++ ****
	opt	- -	- -	++ ***	++ ***	++ ***	++ ***
Hypothalamus	st	+ -	+ -	++ ****	++ ****	++ ****	+++ ****
	bnst	- -	- -	++ **	++ **	++ ***	++ ***
	LPO	- -	- -	+ *	+ *	+ *	++ *
	LH	- -	- -	+ *	+ *	+ *	+ *
	MTu	- -	- -	+ *	+ *	++ *	+ *
	MPOA	+ *	+ *	+++ ***	+++ ***	++++ ***	++++ ***
	DM	- -	- -	++ **	++ **	++ ***	++ ***
	VM	- -	- -	++ **	+ **	++ ***	++ ***
	PVN	- -	- -	+ **	+ **	++ ***	++ ***